INORGANIC CHEMISTRY

FRONTIERS

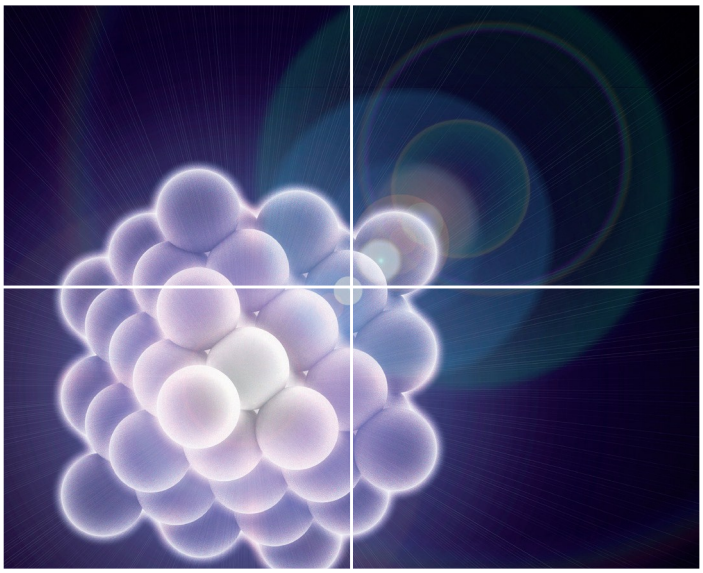

Accepted Manuscript

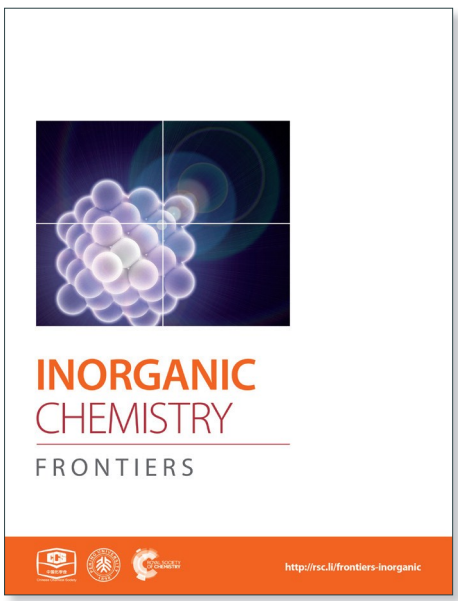

This is an *Accepted Manuscript*, which has been through the Royal Society of Chemistry peer review process and has been accepted for publication.

Accepted Manuscripts are published online shortly after acceptance, before technical editing, formatting and proof reading. Using this free service, authors can make their results available to the community, in citable form, before we publish the edited article. We will replace this *Accepted Manuscript* with the edited and formatted *Advance Article* as soon as it is available.

You can find more information about *Accepted Manuscripts* in the **Information for Authors**.

Please note that technical editing may introduce minor changes to the text and/or graphics, which may alter content. The journal's standard **Terms & Conditions** and the **Ethical guidelines** still apply. In no event shall the Royal Society of Chemistry be held responsible for any errors or omissions in this *Accepted Manuscript* or any consequences arising from the use of any information it contains.

Journal Name

ARTICLE

Rational Design of Semiconductor-based Photocatalysts for Advanced Photocatalytic Hydrogen Production: the Case of Cadmium Chalcogenides

Received 00th January 20xx,
Accepted 00th January 20xx

DOI: 10.1039/x0xx00000x

www.rsc.org/

You Xu,[a] Yi Huang[a,b] and Bin Zhang[a,b]*

Semiconductor-based photocatalytic hydrogen (H_2) production from water has recently received considerable attention because of its enormous promising potentials for solving worldwide ever-increasing energy crises and environmental issues. Among various semiconductors, cadmium chalcogenides (CdX, X = S, Se, Te) with a variety of superior properties including appropriate bandgaps for visible-light absorption, proper conduction band edge potentials for water reduction and abundant reserves on the earth, have fuelled up great interests to explore their photocatalytic properties for solar-driven hydrogen production from water. This review article summarizes the recent progresses in developing CdX-based photocatalyst systems for the production of H_2 from solar water splitting. The basic mechanistic fundamentals of CdX photocatalysts and various strategies to enhance the activity and stability of this class of phcatalysts were introduced in detail. Finally, some key scientific issues and prospective directions in this area of research are also discussed.

1. Introduction

Rising global energy demands, rapidly diminishing reservoir of traditional fossil fuels and ever-increasing environmental concerns have motivated the serious requirements for clean and renewable energy sources.[1-5] Hydrogen (H_2), with the relative abundant of its source of generation, high density of energy (122 kJ/g) and environmental friendliness, is regarded as an attractive and alternative energy carrier without CO_2 emissions.[6-8] Currently, H_2 used in industry is mainly obtained from non-renewable fossil sources by means of steam reforming or coal gasification processes. However, the production process based on this pathway is usually complex, expensive, environmentally hazardous and unsustainable, not to mention the generation of greenhouse gases (CO_2) as a by-product. Recently, splitting water for H_2 production using solar energy has received much attention due to the fact that it could convert sustainable solar energy into storable chemical renewable fuel (H_2), which provides a promising solution to the worldwide ever-increasing energy crises and environmental issues. Approaches for solar water splitting mainly include thermochemical water splitting, photobiological water splitting, photochemical or photocatalytic water splitting and photoelectrochemical or photoelectrocatalytic water splitting. Among these approaches, photochemical water reduction for H_2 production using semiconductor-based photocatalyst systems, which could utilize solar energy to drive a thermodynamic uphill reaction to generate molecule H_2, is a focus of great attention.

Since the pioneering discovery of photoelectrochemical water splitting on TiO_2 photoanode by Honda and Fujishima in 1972,[9] the technology of semiconductor-based photocatalytic water splitting has undergone a considerable development and numerous active semiconductor-based photocatalyst systems have been explored in this important field. In general, the photocatalytic materials for water splitting are required to perform at least two fundamental functions: light harvesting of the maximal possible part of the solar energy spectrum and a catalytic function of efficient water decomposition into O_2 and H_2. Thus, to efficiently utilize solar energy for photocatalytic H_2 production from water, an ideal semiconductor material should meet at least three requirements: an appropriate bandgap for solar energy absorption, proper conduction band position for water reduction, and good stability under the required reaction conditions.

Generally, H_2 and/or O_2 generation from water using solar energy and semiconductor materials can be achieved by means of two different kinds of systems: photoelectrochemical water splitting systems (including single-photoelectrode and dual-photoelectrode systems) and photocatalytic water splitting systems (including half-reaction and overall water splitting systems). In brief, the basic principle of photoelectrochemical water splitting is based on the conversion of solar energy into electricity, which is then used for water electrolysis, within a photoelectrochemical cell involving two electrodes immersed in an electrolyte solution.

[a]Department of Chemistry, School of Science, Tianjin University, Tianjin 300072, China.
[b]Collaborative Innovation Center of Chemical Science and Engineering (Tianjin), Tianjin 300072, China.
E-mail: bzhang@tju.edu.cn

In this case, at least one electrode is made of a semiconductor which is able to efficiently absorb the sunlight and generate photoexcited charge carriers. There are three options for the arrangement of photoelectrodes in the assembly of photoelectrochemical cells for water splitting reaction: (i) a n-type semiconductor as the photoanode and a metal counter electrode (usually Pt); (ii) a p-type semiconductor as the photocathode and a metal counter electrode (usually Pt); (iii) a n-type semiconductor as the photoanode and a p-type semiconductor as the photocathode. In photoanodes made of n-type semiconductors, photogenerated holes accumulate on the surface of the n-type semiconductor and could be used to oxidize water to generate O_2 (if its valance band edge is more positive than the O_2 evolution potential), while electrons are transferred to the counter electrode via the back contact and an external circuit, and used for H_2 evolution reaction (Case i). On the other hand, photocathodes made of p-type semiconductors could utilize photogenerated electrons for H_2 evolution when its conduction band edge is more negative than the H_2 evolution potential; simultaneously, the holes are transferred over the external circuit to the counter electrode for O_2 evolution (Case ii). Alternatively, a photoanode and a photocathode can be connected in tandem to generate a dual-photoelectrode system (Case iii). With the help of the external electric field, which facilitates the charge carrier separation, largely reduces the recombination possibility of charge carriers photoelectrochemical systems usually exhibit relatively high efficiency for water splitting.

Compared to photoelectrochemical systems, the main advantages of photocatalytic water splitting systems are their simple operation and low cost. Photocatalytic water splitting systems could be divided into two types: single photocatalyst systems and Z-scheme systems. A semiconductor material could work as a photocatalyst for photocatalytic H_2 and/or O_2 production from water if it meets all the requirements (e.g. band gap, band edge positions). Note that single photocatalyst overall water splitting system under visible light is one of the greatest challenges in the fields of water splitting. In most cases, water reduction or oxidation half-reactions are studied in this type of systems in the presence of proper sacrificial reagents for H_2 or O_2 generation. Alternatively, two semiconductors can be connected (in series with reversible redox shuttles in some cases) to construct Z-scheme systems, which could achieve the overall water splitting.

Concerning the mechanisms of the reactions, the principle of photocatalytic water splitting is similar to that of photoelectrochemical water splitting. The essential difference between the two consists of the location of the sites of the surface reactions. In the photoelectrochemical process, H_2- and O_2-evolution reactions take place at two spatially separated electrodes. In the photocatalytic process, both oxidation and reduction occur on the surface of the photocatalyst, which exhibits the functions of both anode and cathode. The practical difference between photocatalytic and photoelectrochemical water splitting is that the latter results in both O_2 and H_2 evolving separately, while, in the former, a mixture of both gases is evolved. Moreover, as the photoelectrochemical reactions on photoelectrodes are driven by photoexcited minority carriers, the material selection for constructing photoanode and photocathode is limited not only by their band gap and band edge positions but also their intrinsic conductivity characteristics (n-type or p-type). Differing from photoelectrochemical water splitting process, both n-type and p-type can work as photocatalysts for photocatalytic water splitting when their band gap and band edge positions meet the requirements. This review is focused on the development of photocatalytic systems for H_2 generation.

Among various promising ones under investigated, cadmium chalcogenides (CdX, X= S, Se, Te) are regarded as good candidates for photocatalytic H_2 production because of their following superior characteristics:[10-12] (1) CdX are visible-light-responsive semiconductors which enable them to absorb solar energy across a broader spectrum than these UV-adsorbing semiconductors; (2) CdX nanocrystals possess excellent light-haevesting characteristics, with molar absorptivities of about 10^5-10^7 M^{-1} cm^{-1}; (3) their bandgaps, redox potentials and absorption spectra, which largely determine their photocatalytic properties, can be tuned by controlling a series of structural parameters such as composition, size, shape and morphology; (4) they can be surface-functionalized with a rich variety of ligands, which not only enable them possess either hydrophilic or hydrophobic property but also provides selectivity of functional groups for interaction with other materials. One can see that CdX materials, which has been extensively studied for photocatalytic H_2 generation and which we extensively refer to in this article, indeed belongs to the potential abundant and useful water splitting materials, even though there are environmental and toxicity concerns on potentially harmful release of cadmium.

During the past four decades, significant interest and considerable efforts have been directed to the development of CdX-based materials as photocatalysts for visible-light-driven H_2 generation due to their unique physical, chemical and optical properties. To date, numerous successful achievements have demonstrated their significant applications in photocatalytic H_2 production, while recent great progress in material science and nanotechnology has also greatly accelerated the evolution of this field. Up till now, many excellent earlier and recent review articles have been published by several research groups to summarize the achievements and advances in the field of semiconductor-based photocatalytic water splitting.[13-27] However, there is no one review focusing on CdX-based photocatalysis for H_2 production. Therefore, a timely review to systematically summarize the related progresses and advances about CdX-based photocatalytic H_2-evolution systems is highly desirable. In this review article we will first describe the basic mechanistic fundamentals of CdX-based photocatalysts. We will then discuss the various approaches to improve the photocatalytic performance of various kinds of CdX-based photocatalysts. The synthetic procedures, structural features and photoactivity enhancement mechanism are discussed

based on some representative and important examples. In particular, the focus will be on the relationship between the structural characteristics and features of photocatalysts and their photocatalytic performance. Finally, some key scientific issues as well as prospective directions are also discussed.

2. Some concerns on mechanistic fundamentals of CdX-based photocatalysts.

Semiconductor-based photocatalysis is defined as the chemical reaction induced by photoirradiation in the presence of one or more semiconductors as the catalysts, or more specifically, the photocatalysts. Basically, as illustrated in **Fig. 1a**, semiconductor-based photocatalysis for the splitting of water into H_2 and O_2 involves following three major steps: (i) semiconductor absorbs solar energy and generates mobile charge carriers; (ii) photogenerated charge separation and diffusion from the photogenerated center to the semiconductor's surface; (iii) charge utilization for water reduction or oxidation on the photocatalyst surface. The first two steps (i and ii) relate to the photon absorption and charge carrier transfer in the semiconductor, which are analogous to the photovoltaic process, and the last step (iii) is carrier-induced surface reactions. In a semiconductor-based photocatalysis process, the intrinsic properties of the semiconductor materials fundamentally determine the overall efficiency of the photocatalytic reaction.[13] Generally, the light-absorbing capability of semiconductor materials largely depends on their band gap. The semiconductors with a wider band gap can only utilize the parte of solar energy in UV or near UV regime, while those with a narrower band gap can respond to visible light. From the perspective of solar energy utilization, those visible-light-responding semiconductor materials are more promising photocatalysts as they can utilize solar energy more efficiently. Theoretically, the minimum band gap of semiconductor materials for water splitting reaction appears to be 1.23 eV according to the redox potential of H^+/H_2 and O_2/H_2O redox pairs. In addition to this minimum thermodynamic requirement, additional kinetic overpotential associated with the electron transfer processes and gas evolution step due to the energy losses should be taken into account.[28] Therefore, a much larger band gap (usually > 2.0 eV) of semiconductor is often required for practical photocatalytic systems. Besides the band gap, the positions of the valence band (VB) and conduction band (CB) of semiconductors, which determine the reduction and oxidation power of photogenerated carriers, are also important for the process of photocatalytic water splitting. Specifically, for H_2 production from photocataltic water-splitting, the bottom of CB should be higher (more negative) than the hydrogen evolution potential (+0 V vs. normal hydrogen electrode at pH 0), while the top of VB should be lower (more positive) than the water oxidation potential (+1.23 V vs. normal hydrogen electrode at pH 0) for water-splitting O_2 production.[13,16] Among the CdX semicodncutors, CdS and CdSe are n-type semiconductors with direct bandgaps of ~2.5 and ~1.7 eV, respectively, while CdTe is a p-type semiconductor with a direct bandgap energy of ~1.4 eV (Fig. 1b). From a thermodynamics perspective, CdX semicodncutors are promising candidates for photocatalytic water reduction because they possess more negative CB potential compared to reduction potential of water. In addition, their electronic band structure and the positions of CB and VB can be finely tuned by modifying their crystal structure, composition and morphology.[29] Numerous research results have demonstrated that precise engineering of material-composition and -structure can lead to improved light-harvesting efficiency or/and enhanced reduction/oxidation abilities of the photogenerated carriers, which finally results in an improved photocatalytic activity.

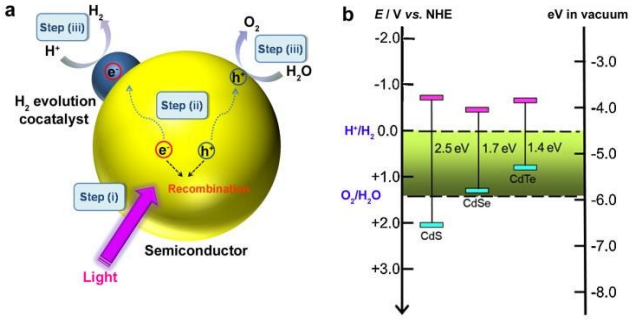

Fig. 1 (a) Illustration for the main processes in semiconductor-based photocatalytic water splitting for H_2 and O_2 evolution. (b) Relationship between band structure of CdS, CdSe and CdTe semiconductors and redox potentials of water splitting (pH = 0).

After excited charges are generated upon light absorption by semiconductor, efficient charge separation and fast charge transport are fundamentally important for semiconductor-based photocatalysis. During step (ii), the recombination of the photogenerated charge carriers inside CdX photocatalyst competes with charge separation/migration process, which largely affects the overall efficiency of photocatalytic reaction. Charge recombination in step (ii) can occur via different mechanisms, including radiative and nonradiative recombiation.[15] It is well recognized that crystal structure, crystallinity, and particle size of the semiconductor materials strongly affect the step (ii). Currently, considerable efforts have been made to increase the separation efficiency and to reduce the recombination probability of photoexcited charge carriers in CdX-based photocatalysts. One popular strategy is structure and morphology control, that is, to develop novel CdX-based photocatalysts with controlled structures and morphologies. Another promising option is to integrate the CdX with other materials to form heterogeneous photocatalysts. When carefully designed, some photocatalytic behaviours, including the mobile direction, the diffusive distance, and the recombination rate of photogenerated charge carriers in these CdX-based heterogeneous photocatalyst systems comprising two or more materials or phases could be well-controlled. Beside these two strategies, another alternative strategy for the extraction of photogenerated electrons from the CdX semicodncutor to reduce the recombination probability of photogenerated carriers is the hybridization of CdX with carbon-based

materials (such as carbon nanotube, graphene). Taking the advantages of carbon-based materials, this kind of CdX-based composites can exhibit improved photoactivity.

It should be emphasized that, even if the separated photogenerated charge carriers possess thermodynamically sufficient potential for H_2- and O_2-evolution reactions, they may recombine if there are no suitable active/reaction sites available on the photocatalyst surface. Therefore, the surface chemical reactions in step (iii), which are driven by photogenerated carriers, are crucial for achieving high efficiency in charge utilization. Water molecules in contact with the semiconductor surface can be reduced to form H_2 by photoelectrons from the CB and oxidized to form O_2 by photoholes from the VB, if the energetic positioning of the bands matches the redox potentials of water reduction and oxidation. It is well recognized that loading proper cocatalysts on photocatalysts' surface could promote or accelerate the surface chemical reactions.[17,18,30] On one hand, cocatalysts could serve as the active reaction sites where H_2- or O_2-ecolution reactions occur. On the other hand, cocatalysts could facilitate the charge separation and reduce the overpotential and activation energy of H_2- or O_2-evolution reductions. Additionally, cocatalysts could enhance the photostability of semiconductor photocatalysts. So far, many kinds of materials including metals, inorganic compounds, hydrogenases, molecular complexes, have been employed as cocatalysts to promote or accelerate the surface redox reactions of CdX-based photocatalysts. Some of them display a high efficiency and good robustness to significantly enhance the photocatalytic H_2 evolution activity of CdX-based photocatalyst systems.

Apart from the above mentioned aspects, photocorrosion, which results from hole-driven oxidation reactions, is another important issue for CdX-based photocatalysts. Taking CdS as an example, S^{2-} in CdS rather than water molecule is oxidized by photogenerated holes accompanied with elution of Cd^{2+} ions in aqueous media when long-term exposed to visible light,[12,16,31] according to Equation (1). Photocorrosion is a critical drawback of CdX photocatalysts, which seriously limits their practical applications in photocatalysis. Sacrificial electron donors are often needed to consume the photongenerated holes or provide electrons for proton reduction when using CdX semicodncutors for photocatalytic H_2 produciton from water. Frequently used hole scavenger materials in CdX-based photocatalytic H_2-evolution systems involve lactic acid, mixture of sulphide and sulphite, ascorbic acid, tertiary amines, triethanolamine and alcohols.

$$CdS + 2h^{+} \rightarrow Cd^{2+} + S \qquad (1)$$

Taken these mechanistic fundamentals into account, an efficient and stable photocatalysts system based on CdX semiconductors should achieve high efficiency in visible-light harvesting, facilitate the photogenerated charge carrier separation and transfer and effectively prevent charge recombination, meanwhile efficiently suppress the photocorrosion and possess a good photostability. Synthetic advancement makes it possible to design and synthesize the desired nanostructures and nanomaterials with particular band alignment favouring expected charge separation. During the last decades, extensive efforts have been made to enhance the photocatalytic activity and stability of CdX semiconductors. The important and representative strategies will be discussed in detail in the following section based on some selective examples.

3. Strategies for enhancing the photocatalytic performance of CdX

3.1 Modifying the crystal structure and morphology of CdX

Bulk CdX materials alone demonstrate low photoactivity and poor stability for H_2 photogeneration, mainly due to the rapid surface/bulk recombination of photogenerated electrons and holes and large H_2 production activation energy or overpotential. Compared to their bulk counterparts, CdX materials in nanoscale show more promising potentials for photocatalytic applications owing to their unique properties and advantages. Firstly, the decrease in particle size usually could directly result in an increase of the surface area and active reaction sites, both of which are important for surface chemical reactions. Secondly, reducing the particle size of a photocatalyst could shorten the diffusion pathway of the photogenerated charge carriers, leading to decreased recombination probability. Thirdly, making semiconductor materials in the form of nanoparticles allows us to utilize quantum confinement effect for both opening their bandgap and for adjustment of their energy levels. Furthermore, investigations have revealed that the separation and migration of photogenerated charge carriers are strongly affected by the crystal and structural features of the materials (*e.g.* crystallinity) and a series of surface properties including particle size, surface area, surface structure and active reaction sites, etc.[13] By tuning these parameters, the properties of a semiconductor material such as the bandgap, the CB and VB positions can, in principle, be tailored to enhance its activity and stability in photocatalytic H_2 production application.[32-42]

3.1.1 Modifying the crystal structure of CdX

The crystal structure of the semiconductor plays an essential role in determining its photocatalytic properties. It is well recognized that good crystallinity could lead to significant improvement of the charge carrier separation and migration properties, whereas lattice defects in semiconductors usually operate as trapping and recombination centers for the photogenerated charge carriers, which is not conducive for the photocatalysis. Bao *et al.* reported a facile thermolysis procedure of Cd-thiourea complex to synthesize phase-controlled CdS nanocrystals for photocatalytic H_2 production.[32] This study showed that the photocatalytic activity for H_2 production over CdS had a direct relationship with phase structure and phase composition, and the pure hexagonal CdS had the highest photocatalytic activity among the different phases of CdS photocatalysts with Pt as the cocatalyst. Li and

co-workers demonstrated that the photocatalytic activity of Pt/CdS system for H_2 evolution can be notably enhanced by suitable photoetching.[33] They clarified that the selective removal of grain boundary defects which acted as charge recombination centers for photogenerated charge carriers can decrease the recombination chance of charge, thus increasing the photocatalytic activity. In a recent example, Wang *et al.* reported the fabrication of facet-engineered CdS nanocrystals by controlling the synthesis kinetics.[34] Growth rate control of {0001} facets (r_1) and {$10\bar{1}1$} facets ($r_{1'}$) of CdS nanocrystals was achieved by simply employing a syringe pump, which enables them to finely tune the crystal shape from nanocones, to nanofrustums, and further to nanoplates (Fig. 2a). Study on their photocatalytic activities revealed that the CdS nanoplates with largest {0001} facets exhibited the highest photocatalytic activity for H_2 production in comparison to the nanocones and nanofrustums (Fig. 2b).

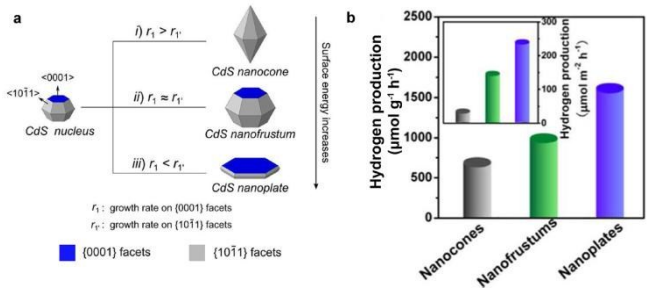

Fig. 2 Schematic illustration of the formation of a CdS nanocone, a CdS nanofrustum, and a CdS nanoplate, simply controlled by adjusting Cd^{2+} injection rate. (b) Average photocatalytic H_2 production rate of various CdS nanostructures. Inset in (b) shows corresponding specific activities that were normalized with respect to their calculated surface areas. Reproduced with permission from ref. 33. Copyright 2015 American Chemical Society.

3.1.2 Modifying the size and morphology of CdX

Besides the crystal structure, size and morphology are also important surface properties affecting the photocatalytic properties of CdX materials. For example, Zhu and co-workers have synthesized various CdS nanostructures with controlled morphologies (nanorods and nanospheres) and compared their photocatalytic activity for H_2 production.[35] They found the one-dimensional CdS nanorods (~10 nm in diameter and ~200 nm in length), which could be prepared by using diethylenetriamine(DETA) as template and coordination agent, exhibited higher photocatalytic H_2 generation activity than other CdS nanostructures. They attributed the favorable photocatalytic performance of these CdS nanorods to the anisotropic characteristic and good dispersion, which led to excellent separation ability of photogenerated charge carriers. In another similar example, Osterloh *et al.* have demonstrated CdSe nanoribbons showed enhanced photocatalytic activities toward H_2 production when compared to bulk CdSe counterparts.[36] Recently, we synthesized ultrathin CdS nanosheets and studied their photocatalyic activity toward H_2 generation.[37] In this case, the ultrathin CdS nanosheets with a thickness of ~4 nm were prepared through an ultrasonication-induced aqueous exfoliation approach using CdS-DETA hybrid nanosheets as starting materials (Fig. 3a). Fig. 3b shows the transmission electron microscopy (TEM) image of the ultrathin CdS nanosheets. Study of their photocatalytic activity demonstrated that these ultrathin CdS nanosheets exhibited much higher H_2 production rate than CdS nanoparticles, CdS aggragates, as well as the pristine CdS-DETA hybrid nanosheets. The enhancement in photocatalytic activity could be ascribed to their unique ultrathin morphology and single-crystal-like structural feature which can not only provide huge surface area and more active sites, but also lead to the shift of CB to a higher position and facilitate the separation of the photogenerated charge carriers. Very recently, our group described the synthesis of 3D hierarchical ultrathin-branched CdS nanowire arrays (3DHU-CdS) and their application for photocatalytic H_2 evolution.[38] In this study, the 3DHU-CdS with an adjustable branch size could be synthesized by means of a facile chemical transformation strategy using 2D ZnS–amine inorganic–organic hybrid nanosheets as the precursor (Fig. 3c,d). We found the obtained 3DHU-CdS exhibited enhanced photocatalytic activity for visible-light-driven H_2 generation from water due to their unique hierarchical and ultrathin structural features. Peng et al. described the flower-like CdSe architectures composed of ultrathin nanosheets for enhanced visible-light-driven photocatalytic H_2 production.[39]

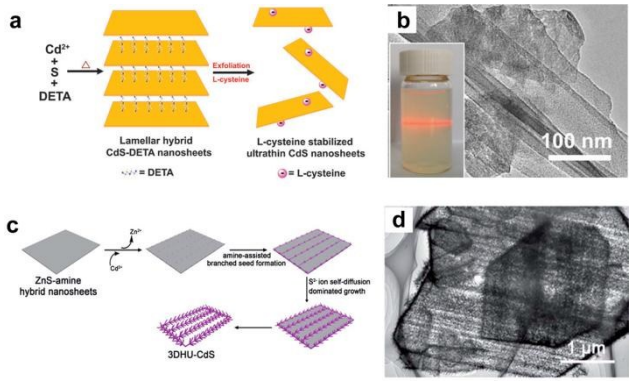

Fig. 3 (a) Schematic illustration of the preparation of L-cysteine stabilized ultrathin CdS nanosheets. (b) TEM image of ultrathin CdS nanosheet and the corresponding colloidal CdS diepersion displaying Tyndall effect. (c) Schematic illustration of the preparation of 3D hierarchical ultrathin-branched CdS nanowire arrays. (d) TEM image of the 3D hierarchical ultrathin-branched CdS nanowire arrays. (a,b) Reproduced with permission from ref. 37. Copyright 2013, The Royal Society of Chemistry. (c,d) Reproduced with permission from ref. 38. Copyright 2015, The Royal Society of Chemistry.

Several research groups have investigated the size-dependent performance of CdX materials in the photocatalytic H_2 evolution. The work by Sathish *et al.* showed that CdS particles in nanometer scale could display a higher photocatalytic activity for H_2 generation compared to bulk CdS counterparts.[40] In a recent example, Osterloh and co-workers provided the first quantitative analysis of quantum-size-controlled photocatalytic H_2 evolution at the semiconductor (CdSe)-solution interfaces.[41] Based on their results, it was found that the H_2 evolution rate from illuminated suspended CdSe quantum dots (QDs) in aqueous Na_2SO_3 solution was dependent on the size of CdSe nanocrystals. The study by Grigioni *et al.* also demonstrated the size-dependent

performance of CdSe QDs in the photocatalytic evolution of H_2 under visible light irradiaotion.[42] They found the 2.8 nm-sized CdSe samples exhibited the highest H_2 production rate due to their good visible light harvesting capability, suitable conduction band position and low probability of photogenerated charge carrier recombination.

It must be realized that despite numerous evidences have demonstrated the feasibility in the photocatalytic water splitting using pure CdX semiconductor nanomaterials, their H_2 evolution rates and the quantum efficiencies (QEs) are still too low to be able to efficiently utilize solar energy even though in the presence of sacrificial agents. Therefore, many research efforts have been directed to improve their photocatalytic properties by modifying CdX with other materials through a series of approaches to further modify their activity and stability.

3.2 Forming CdX-based solid solutions

Forming solid solution is an efficient composition-engineering strategy to modify the photocatalytic properties of CdX semiconductor materials. Compared to the pristine CdX materials, solid solutions possess some unique advantages such as tunable absorption properties in the visible region of the solar spectrum, controllable band structure and better electrical conductivity with the help of insert metals (M), leading to enhanced visible-light response and improved photoactivity.

$Cd_xZn_{1-x}S$ (0<x<1) solid solution, formed by combining semiconductor ZnS with wide bandgap and semiconductor CdS with narrow bandgap, has attracted much research interest for visible-light-driven photocatalysis applications.[43-51] For exampe, our group have synthesized nanoporous single-crystal-like $Cd_xZn_{1-x}S$ nanosheets with tunable pore size and composition by the cation-exchange reaction of inorganic-organic hybrid ZnS-DETA nanosheets with Cd^{2+} ions and demonstrated their high photocatalytic activity for H_2 production.[43] **Fig. 4a** displayed the typical scanning electron microscopy (SEM) image of the porous $Cd_{0.5}Zn_{0.5}S$ nanosheets. we demonstrated the porous $Cd_{0.5}Zn_{0.5}S$ nanosheets showed a stable H_2 production rate of about 0.5 mmol h^{-1}/0.3 g catalyst, which is about 2.5 times than that of $Cd_{0.5}Zn_{0.5}S$ nanorods (**Fig. 4b**). In another example, Guo, Yao and co-workers have synthesized $Cd_xZn_{1-x}S$ solid solution with nano-twin structures through a precipitate-hydrothermal method and evaluated their photocatalytic activity for H_2 evolution.[44] Their study results revealed that such $Cd_xZn_{1-x}S$ nanocrystal photocatalysts showed a higher photocatalytic H_2 production activity compared to the pristine CdS counterpart. Among them, $Cd_{0.5}Zn_{0.5}S$ photocatalysts showed the highest activity with a H_2 evolution rate of 1.79 mmol h^{-1}/0.1 g catalyst and an apparent QE of 43% at 425 nm.

Investigations demonstrate that the photocatalytic performance of $Cd_xZn_{1-x}S$ solid solution can be further improved by doping with some transition metal ions, such as Cu,[45,46] Ni,[47] Sn,[48] and La[49]. For example, Liu *et al.* have successfully synthesized a Cu doped $Cd_{0.1}Zn_{0.9}S$ photocatalyst by a coprecipitation method, and an apparent QE of about 9.6% can be achieved by the $Cd_{0.1}Cu_{0.01}Zn_{0.89}S$ photocatalyst without any cocatalyst at 420 nm.[45] Chen and co-workers reported an efficient strategy for the enhancement of photocatalytic H_2 evolution in which La was successfully doped into the depletion layer of the $Cd_{0.6}Zn_{0.4}S$ photocatalyst via a facial solvothermal method.[49] Apart from metal doping, non-metal doping is another effective approach to modify the photocatalytic properties of semiconductors. One successful case is doping various nonmetal anions (such as C, N, S, etc.) onto TiO_2 to modify its optical and photocatalytic properties,[52,53] which should open up interesting possibilities to modify the photocatalytic properties of CdX semiconductors by proper nonmetal ion doping.

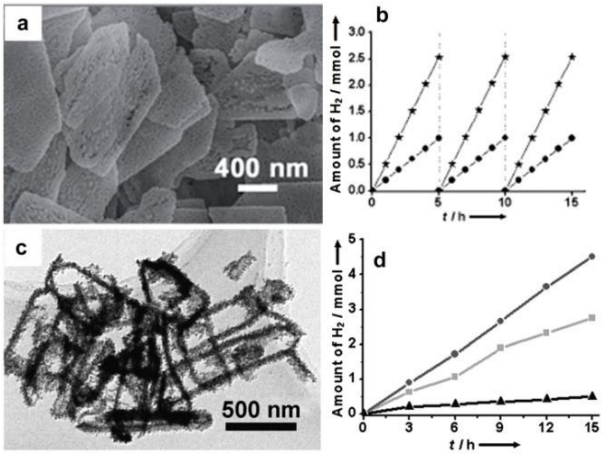

Fig. 4 (a) SEM image of porous $Cd_{0.5}Zn_{0.5}S$ nanosheets. (b) Time course of evolved H_2 under visible-light irradiation of $Cd_{0.5}Zn_{0.5}S$ porous nanosheets (★) and $Cd_{0.5}Zn_{0.5}S$ nanorods. (c) TEM image of hollow $Cd_{0.33}Zn_{0.67}Se$ nanoframes. (d) Time course of evolved H_2 under visible-light irradiation of hollow $Cd_{0.33}Zn_{0.67}Se$ nanoframes(●), hollow $Cd_{0.25}Zn_{0.75}Se$ nanoframes(■), and $Cd_{0.33}Zn_{0.67}Se$ nanoparticles (▲) . (a,b) Reproduced with permission from ref.43. Copyright 2012, John Wiley and Sons. (c,d) Reproduced with permission from ref. 56. Copyright 2012, John Wiley and Sons.

Except for $Cd_xZn_{1-x}S$, other CdX-based solid solutions such as $Cd_xMn_{1-x}S$[54], $CdIn_2S_4$[55], $Cd_xZn_{1-x}Se$[56], are also found to possess efficient photocatalytic activity. For example, Ikeue and co-workers have successfully fabricated $Cd_xMn_{1-x}S$ photocatalyst through a hydrothermal method.[54] They found that the high photocatalytic activity for H_2 evolution of this $Cd_xMn_{1-x}S$ photocatalyst was caused by low-crystalline character. Moreover, they demonstrated this $Cd_xMn_{1-x}S$ photocatalyst showed better tolerance to photocorrosion compared to pure CdS counterpart. The study by Kale et al. showed the efficient photocatalytic H_2 production over nanostructured $CdIn_2S_4$.[55] As an example for the study on $Cd_xZn_{1-x}Se$ solid solutions, our group synthesized hollow $Cd_xZn_{1-x}Se$ nanoframes via a selectively cation-exchange strategy and demonstrated their composition-dependent photocatalytic activity for H_2 production.[56] **Fig. 4c** showed the typical TEM image of the hollow $Cd_{0.33}Zn_{0.67}Se$ nanoframes. They found that the $Cd_{0.33}Zn_{0.67}Se$ nanoframes showed an obviously higher H_2 production rate than that of $Cd_{0.25}Zn_{0.75}Se$ nanoframes and $Cd_{0.33}Zn_{0.67}Se$ nanoparticles (see **Fig. 4d**).

Apart from the component (the choice of insert metals (M), the composition (the ratio of M to Cd) of the solid solution can also influence the band energy level and thus the photocatalyic properties.[57,58] For example, Yu and Guo *et al.* have revealed that the bandgap effect of composition-tunable $Cd_xZn_{1-x}S$ solid solutions on the superior photocatalytic H_2 evolution.[57] They found that the Zn/Cd molar ratio in these $Cd_xZn_{1-x}S$ solid solutions could largely affect the band structure and positions and their final photocatalytic activity of the resulted solid solution photocatalysts. Among various $Cd_xZn_{1-x}S$ solid solutions, the $Zn_{0.5}Cd_{0.5}S$ sample presented the highest H_2-production rate (7.42 mmol h^{-1} g^{-1}), which was about 24 and 54 times higher than that of the pure CdS and ZnS samples, respectively. The activity of $Zn_{0.5}Cd_{0.5}S$ was even higher than that of the optimal Pt-loaded CdS sample (see **Fig. 5**).

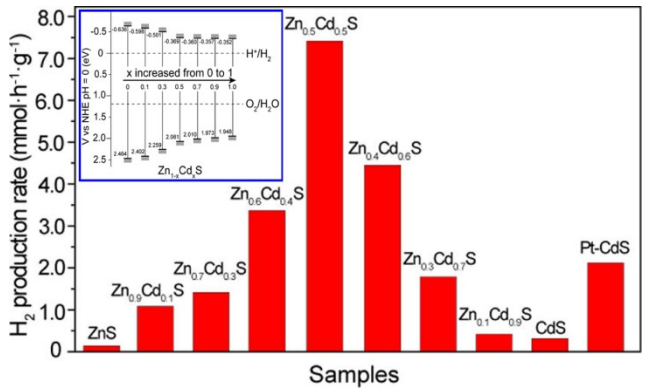

Fig. 5 Comparison of the photocatalytic activities of the $Zn_{1-x}Cd_xS$ samples with different compositions and Pt (0.9 wt%)/CdS sample for the photocatalytic H_2-production from 0.44 M Na_2S and 0.31 M Na_2SO_3 mixed aqueous solution under visible-light irradiation. The inset is the conduction and valence band edge potentials of $Zn_{1-x}Cd_xS$ samples with different compositions. Reproduced with permission from ref. 57. Copyright 2013 American Chemical Society.

3.3 Loading cocatalysts onto CdX

As discussed above, loading proper cocatalysts on the semiconductor photocatalyst could effectively promote or accelerate the surface chemical reactions.[17,18,30] Generally, the cocatalysts for semiconductor-based photocatalytic water splitting can be divided into two categories according to their different functions, that is, H_2-evolition cocatalysts and O_2-evolution cocatalysts. In this section, we focus on the development of the combination of H_2-evolution cocatalysts with CdX-based photocatalysts for photocatalytic H_2 generation.

3.3.1 Metal cocatalysts

Noble metals, such as Pt,[32,33,40,59-78] Au,[63,74] Ru,[76,79] Pd,[74,80] and Rh,[81,82] have been widely used as efficient H_2-evolution cocatalysts in combination with CdX semiconductor photocatalysts by forming metal/CdX heterogeneous photocatalysts, with some representative examples summarized in **Table 1**. Among them, Pt, with its large work function and low overpotential for H_2 evolution reaction, is one of the most effective and most investigated H_2-evolution cocatalyst. Excellent H_2 production rates and QEs from various Pt/CdX heterogeneous photocatalysts have been reported by many research groups. In a typical example, Bao *et al.* demonstrated the loading of monodisperse Pt nanoparticles (3~5 nm) onto porous CdS nanostructures could remarkably improved their photocatalytic activity for H_2 evolution.[59] Study on the photocatalytic performance showed the pure nanoporous CdS nanostructures exhibited a H_2 evolution rate of 0.13 mmol $h^{-1}g^{-1}$ from the aqueous solution containing Na_2S and Na_2SO_3 as sacrificial reagents under visible-light irradiation, and the H_2 evolution rate increased to 3.67 mmol $h^{-1}g^{-1}$ over (0.5%) Pt/CdS and further to 27.3 mmol $h^{-1}g^{-1}$ over (13%) Pt/CdS, with an apparent QE reaching ~60% at 420 nm. Amirav *et al.* designed and synthesized a three-component well-defined nanoheterostructure composed of a Pt-tipped CdS rod with an embedded CdSe seed.[60] In this photocatalyst system, the photogenerated holes were three-dimensionally confined to the CdSe, whereas the photogenerated electrons were transferred to the Pt tip. Ultimate result was the efficient separation of photogenerated electrons and holes, the decrease of the charge recombination probability, as well as the suppression of photocorrosion of CdS. They found that the activity for H_2 production could be significantly increased compared to that of unseeded nanorods by tuning the length of nanorod heterostructure and the seed size. Study on their photocatalytic activity revealed that the three-component photocatalytic system was not only highly active for H_2 evolution with an apparent QE of 20% at 450 nm, but also active under orange light illumination, and demonstrated improved stability compared to Pt-tipped CdS nanorods without a CdSe seed. Li group have presented a successful example by co-loading of Pt as the reduction cocatalyst and PdS as the oxidation cocatalyst on the CdS photocatalyst.[61] The optimal Pt(0.3wt%)-PdS(0.13wt%)/CdS photocatalyst system could achieve an improved QE of 93% for H_2 production in the presence of Na_2S and Na_2SO_3 as sacrificial agents under visible-light irradiation, which also exhibits excellent stability during the long-term photocatalytic reaction. This QE was close to that of the primary courses of natural photosynthesis. The detailed study indicated that the cocatalysts can effectively prohibit the recombination of electrons and holes and promote the efficient utilization of charges at the shallow trap states of CdS. In a recent important advance, Yu, Jiang and co-workers described a ternary ZnS-(CdS/M) (M = Au, Pd, Pt) nano-architttecture for highly efficient photocatalytic H_2 production.[74] The ternary ZnS-(CdS/M) hybrids were prepared by the post-synthetic modification of binary multi-node sheath ZnS-CdS heteronanorods, which were transformed from single component ZnS nanorods via sequential cation exchange. In such a nano-architttecture, the delivery of photogenerated electrons from the CdS node sheath not only to the metal surface but also to the exposed ZnS stem, promoting the separation of electron and hole carriers, thereby leading to the performance improvement of photocatalytic H_2 evolution(see **Fig. 6**). Tongying *et al.* reported CdSe/CdS/Pt double heterojunction nanowires as efficient photocatalyst system for H_2 generation.[75]

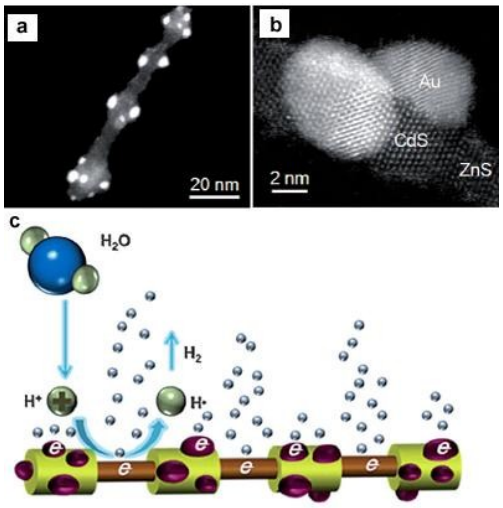

Fig. 6 (a,b) HAADF-STEM images of the ZnS-(CdS/Au) hetero-nanorods. (c) Schematic representation of the photocatalytic generation of H_2 from the hetero-nanorods. Reproduced with permission from ref. 74. Copyright 2015, John Wiley and Sons.

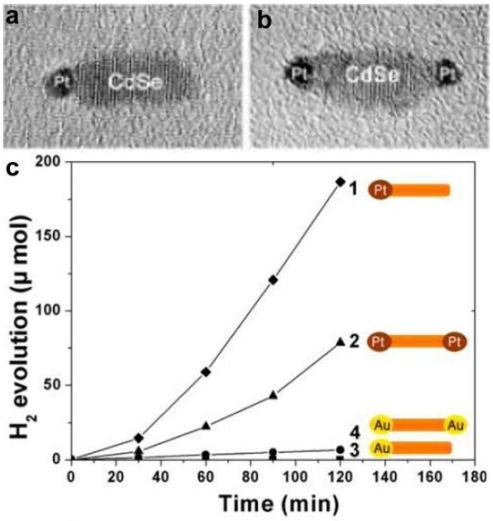

Fig. 7 (a, b) Typical TEM images of single (a) and double (b) Pt-tipped CdSe nanorods. (c) Time course of H_2 evolution by various photocatalysts: single Pt-tipped CdSe (◆), double Pt-tipped CdSe (▲), double Au-tipped CdSe, and single-Au tipped CdSe. Reproduced with permission from ref.63. Copyright 2012 American Chemical Society.

For the cocatalysts loading onto the CdX semiconductors, a series of factors, such as the loading condition, the geometrical configuration of the semiconductors, and the size and composition of the cocatalysts, can largely influence the final effect of the composite catalysts. For example, Xu and co-workers compared the photocatalytic activities of various Pt/CdS photocatalyst systems obtained from different Pt reduction environment for H_2 production and investigated the effect of loading condition for Pt nanoparticles on the surface of CdS photocatalyst.[62] In this study, Pt was deposited on CdS photocatalyst by means of a photoreduction method. They found that the solution environment during Pt photoreduction played an essential role on the activity of the final Pt/CdS photocatalyst system. Study on the photocatalytic activity for H_2 producction from various Pt/CdS photocatalyst systems revealed that the sampe with Pt reduced in NaOH alkaline solution exhibited a markedly higher H_2 evolution activity (13 mmol $h^{-1}g^{-1}$) than that of samples obtained in acidic or neutral solution (0.5 mmol $h^{-1}g^{-1}$) in the presence of Na_2S and Na_2SO_3 as sacrificial reagents. Song *et al.* investigated geometrical (single- or double-tipped) and compositional (Pt or Au) variations of active metal components in a well-defined CdSe nanorod system.[63] In this case, single Pt-tripped, single Au-tripped, double Pt-tripped, and double Au tripped CdSe nanorods could be fabricated by controlling the component and the concentration of Pt (or Au) precursors. Study of their photocatalytic activities revealed that these catalysts exhibited significant dependency of the catalytic activity on the catalytic geometry and the choice of the noble metal tips. They found that the Pt-tripped catalysts showed higher photocatalytic activity than Au-tripped catalysts. Moreover, the H_2 amount of the single Pt-tripped CdSe nanorods was about ~50% larger than that of the double Pt-tripped structure, although the loading amount of Pt in the former was only half of that in the latter (see **Fig. 7**).

Recently, several earth-abundant transitional metals H_2-evolution cocatalysts, such as Ni[83-88] and Co[89], have been used as substitutes for noble metals to enhance the activity of CdX photocatalysts. For example, Wang *et al.* reported the enhanced activity for photocatalytic H_2 generation in the Ni/CdS nanocomposite photocatalysts.[83] In their study, Ni nanoparticles with a high degree of crystallization and an average size of about 10 nm were prepared via chemical reduction of $NiCl_2$ precursor by hydrazine in an aqueous solution followed by loading on CdS nanorods by photo-induced deposi-tion. They found that the loading of Ni nanoparticles could increasethe specific surface area of CdS nanorods. Upon visible light irradiation, the Ni/CdS photocatalysts with a Ni contentof 4 wt% could provide a H_2 evolution rate of 25.8 mmol $h^{-1}g^{-1}$ from $(NH_4)_2SO_3$ aqueous solution with a QE of 26.8% at 420 nm. Moreover, the Ni/CdS nanocompos-ite photocatalyst could retain a high stability and activity evenafter 20 h photocatalytic reaction. Feldmann and co-workers also demonstrated the efficient photocatalytic H_2 production on Ni-decorated CdS nanorods.[84] In this study, the Ni nanoparticles(2~8 nm) were loaded on the surface of the cysteine stabilized CdS nanorods through in situ photodeposition. They employed ahydroxyl anion/radical redox couple (·OH/−OH), which posses agood mobility and can react with CdS and the sacrificial agent(ethanol), to assist in the efficient transfer of the photogenerated hole from the CdS to ethanol (see **Fig. 8**). As a result, a significant enhancement in the H_2 generation rate could beachieved, with an apparent QE of 53% at 447 nm and a remarkable H_2 formation rate of 63 mmol g^{-1} h^{-1} under optimal conditions. Moreover, the obtained photocatalyst exhibited an excellent long-term stability (over 220 h) for photocatalytic H_2 production. The work by Chen et al. showed that metallic Ni can be deposited on CdS by a hydrothermal reduction method with ethylene glycol.[85] The optimal Ni (5 wt%)/CdS photocatalyst gave a H_2

evolution rate of around 3 mmol h^{-1}, which was even higher than that of the Pt(0.5 wt%)/CdS system under the same reaction condition. More recently, Zhukovskyi et al. demonstrated efficient photocatalytic H_2 generation from Ni nanoparticle decorated CdS nanosheets.[86] As an example for loading a Co cocatalyst onto CdX, Wu and co-workers demonstrated a robust catalytst system *in situ* formed from CdTe QDs and $CoCl_2 \cdot 6H_2O$ in aqueous accorbic acid solution for photocatalytic H_2 generation.[89] In this case, the Co^{2+} ions, which were directly bounded to the surface of CdTe QDs, could be photoreduced partially or completely under visible-light irradiation to form a hybrid Co_h-CdTe catalyst system, which could achieve a high H_2 evolution rate of 25 μmol h^{-1} mg^{-1} with a turnover number (TON) of 86 250 respect to CdTe QDs 21 h irradiation.

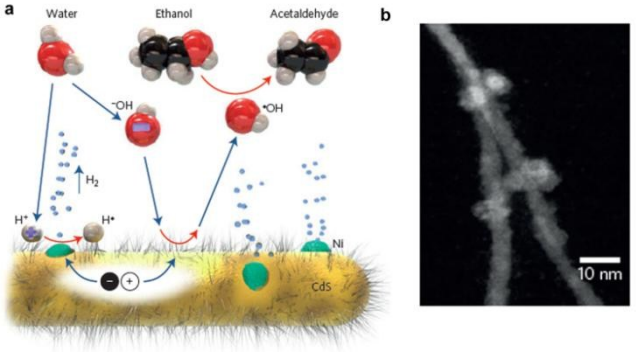

Fig. 8 (a) Schematic of the photocatalytic generation of H_2 from Ni-decorated CdS nanorods under the proposed hole shuttle machansm. (b) HAADF-STEM image of the Ni-decorated CdS nanorods. Reproduced with permission from ref. 84. Copyright 2014, Nature Publishing Group.

3.3.2 Transition metal oxides and hydroxides

Some earth-abundant transition metal oxides, such as NiO,[90] Ni_2O_3,[91] NiO_x,[92] CoO_x,[93] Co_3O_4,[94] and MoO_3,[95] are also well-known as highly active cocatalysts after being integrated with CdX materials for photocatalytic H_2 production, as summarized in **Table 1**.

For example, Chen *et al.* showed that in situ photodeposition of NiO_x on CdS could enhance its photocatalytic H_2 generation activity. They found the environment of deposition could affect the photocatalytic activityof the resultant NiO_x–CdS photocatalyst.[92] The NiO_x–CdS photocatalyst formed in alkaline solution showed the highest activity of photocatalytic H_2 production due to the high dispersion and tight deposition of NiO_x on CdS and better hole transfer in alka-line condition, reaching to 590.8 μmol h^{-1}, which was 117 times higher than that of pure CdS. Yan *et al.* prepared a CoO_x-loaded TiO_2/CdS semiconductor composite by a simple solvothermal method.[93] Study on their photocatalytic behaviour revealed that CoO_x could act as an efficient cocatalyst to enhance the photocatalytic activity of TiO_2/CdS and its content exhibited a significant influence on the activity. The optimal CoOx loading content is determined to be 2.1 wt%, and the average rate of H_2 evolution is 660 μmol g^{-1} h^{-1} in the presence of Na_2S and Na_2SO_3 as sacrificial agents, which is ahout 7 times higher than TiO_2/CdS composite and CdS. The work by Yuan *et al.* showed that Co_3O_4 can serve as efficient H_2-evolution cocatalyst in combnation with CdS semiconductor.[94]

Several metal hydroxides[96-99] and Layered double hydroxides(LDH)[100] have also been developed as efficient and noble metal-free cocatalysts for photocatalytic H_2 production. Jaroniec, Yu and co-workers found the highly efficient photocatalytic H_2 production on the $Ni(OH)_2$-loaded CdS photocatalyst. The optimal $Ni(OH)_2$ (0.23 mol%)/CdS photocatalyst could achievea visible-light H_2-production rate as high as 5085 mol $h^{-1}g^{-1}$ and a QE of 28% at 420 nm.[96] The H_2-production rate on $Ni(OH)_2$-loaded CdS photocatalyst was 145 and 1.3 times higher thanthose of pure CdS and Pt(1 wt%)/CdS photocatalyst, respec-tively. Yan *et al.* demonstrated the use of $Ni(OH)_2$ as an efficient cocatalyst on CdS/reduced graphene oxide (CdS/RGO) composite photocatalyst for visible light-driven H_2 production.[97] The optimal $Ni(OH)_2$(1.0 wt%)/CdS/RGO photocatalyst could give a H_2-production rate of 4731 μmol $h^{-1}g^{-1}$, which is nearly 10 times higher than that of CdS/RGO photocatalyst under the same condition. The work by zhang *et al.* showed that $Co(OH)_2$-modified CdS nanorods exhibited a visible-light H_2-production rate of a H_2 generation rate of 61 μmol h^{-1} g^{-1}, which exceeded that of pure CdS by a factor of 41 times[99] (see **Fig. 9**). The outstanding H_2-evolution activity of $Co(OH)_2$ and interface formed between $Co(OH)_2$ and CdS which facilitates the electron transfer from CdS to $Co(OH)_2$ were thought to be the main reasons for the enhanced photocatalytic activity. Hwang and co-workers prepared strongly coupled Zn-Cr-LDH-CdS nanohybrids through the electrostatically derived self-assembly of cationic Zn-Cr-LDH nanosheets and cationic CdS QDs with anionic linkers.[100] They found the hybridization of CdS with Zn-Cr-LDH leads to significant enhancement of the photocatlaytic activity of CdS for visible-light-induced H_2 generation.

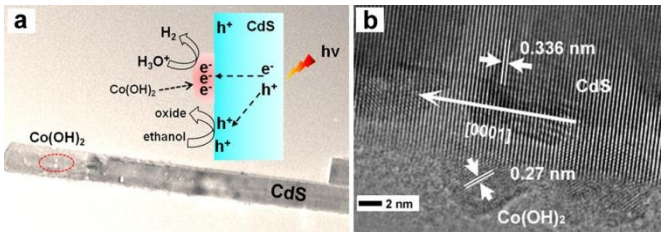

Fig. 9 (a) TEM image and (b) HRTEM image of the $Co(OH)_2$-modified CdS nanorod. Reproduced with permission from ref.99. Copyright 2014, American Chemical Society.

3.3.3 Transition metal sulphides, carbides and phosphides

To date, many transition metal sulphides,[101-123] phosphides[124-129] and carbides[130] have been employed as efficient H_2-evolution cocatalysts to enhance the photocatalytic performance of CdX photocatalysts, as summarized in **Table 1**.

MoS_2 is a well-known cocatalyst for photocatalytic H_2 production, which have been widely investigated on variety of semiconductor photocatalysts. Li and co-workers studied the role of MoS_2 as a cocatalyst loaded on CdS for photocatalytic H_2 production.[101] In this case, the MoS_2/CdS photocatalyst system with highly dispersed MoS_2 on CdS were prepared by

impregnating CdS with an aqueous solution of $(NH_4)_2MoS_4$, followed by a treatment in H_2S flow at high temperatures. This study showed that the activity of CdS can be enormously increased by loading MoS_2 as a cocatalyst, and the activity of MoS_2/CdS photocatalyst system could be even higher than that of Pt/CdS. In another recent example, Zhang and co-workers prepared MS_2-CdS (M = W or Mo) nanohybrids, with single-layer MS_2 nanosheets with lateral size of 4~10 nm selectively grow on the Cd-rich (0001) surface of wurtzite CdS nanocrystals, via a facial one-pot wet-chemical method for photocatalytic H_2 production[109] (**Fig. 10a**). The photocatalytic performance of WS_2-CdS and MoS_2-CdS nanohybrids towards the H_2 production under visible-light irradiation (λ>420 nm) was found to be about 16 and 12 times higher than that of pure CdS, respectively. The enhancement in activity was attributed to the large number of active sites of single-layer MS_2 nanosheets and the inherent p/n heterjunction formed between MS_2 and CdS(**Fig. 10b**). The study by Zong *et al.* also demonstrated that the loading of WS_2 onto CdS could significantly enhance the evolution of H_2 from lactic solution under visible-light irradiation.[110] Alivisatos and co-workers described the coating of amorphous MoS_3 on CdSe-seeded CdS nanorods by means of a facile one-step thermal process.[111] This study showed the maximum H_2-evolution rate could reach 100 mmol h^{-1} g^{-1} with a QE of 10 % at 450 nm.

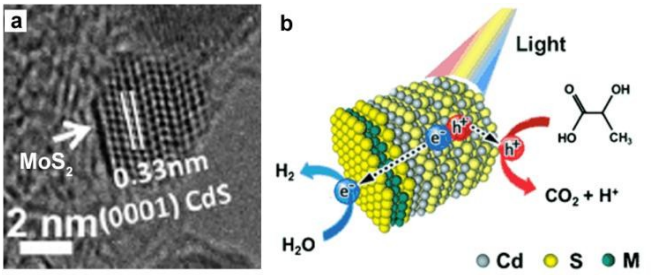

Fig. 10 (c) HR-TEM image of MoS_2-CdS nanohybrids. (d) Schematic illustration of the photocatalytic process of MS_2-CdS nanohybrids in the lactic acid solution. Reproduced with permission from ref. 109. Copyright 2015, John Wiley and Sons.

Besides MoS_2, MoS_3 and WS_2, some other transition metal sulphides, such as NiS,[112-117] NiS_2,[118] CuS[119-121] and CoS[112,117] also can serve as efficient H_2-evolution cocatalysts to boost the photocatalytic activity of CdX photocatalysts. By using a simple hydrothermal route, Xu and co-workers have prepared a NiS/CdS nanocomposite ,with ultrafine NiS nanoparticles deposited on CdS nanoparticle, as highly active photocatalysts for H_2 production.[112] The optimized NiS(1.2 mol%)/CdS photocatalyst could reach a visible-light-driven H_2-evolution rate of 7.27 mmol $h^{-1}g^{-1}$ using lactic acid as a sacrificial agent with a QE of 51.3% at 420 nm, which is even higher than that of Pt(1 wt%)/CdS photocatalyst. They proposed that the loading of NiS cocatalyst not only could efficiently promote the separation and transport of photogenerated electrons from the CB of CdS to the NiS nanoparticlrs but also could accelerate the electrochemical adsorption and desorption kinetics for H_2 evolution through the following reaction equations (2) and (3):

$$NiS + e^- + H^+ \rightarrow HNiS \quad (2)$$

$$HNiS + e^- + H^+ \rightarrow NiS + H_2 \quad (3)$$

The study by Xue and co-workers showed the loading of NiS_2 co-catalyst resulted in remarkable enhancement for H_2 production over the $CdLa_2S_4$ photocatalyst under visible light irradiation.[118] The optimal hybrid photocatalyst with 2 wt% NiS_2 loading exhibited a H_2 production rate of 2.5 mmol h^{-1} g^{-1}, which was more than 3 times higher than that of the pristine $CdLa_2S_4$ photocatalyst. Zhang *et al.* prepared CuS/CdS nanoposites by a simple hydrothermal and cation exchange method and investigated their photocatalytic acitivity for H_2 produciton.[119] They found the loading of CuS as the cocatalyst could remarkably enhanced the photocatalytic performance of CdS. The optimized CuS (3 mol %)/CdS displayed the highest photocatalytic activity, giving an H_2 evolution rate of 332 μmol g^{-1} h^{-1}, exceeding that of pure CdS by 3.5 times.

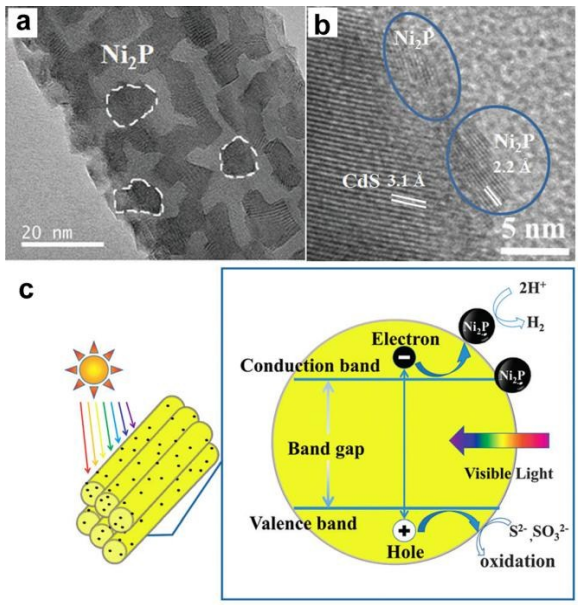

Fig. 11 (a) HRTEM image and (b) high-magnification HRTEM image the Ni_2P/CdS heterostructures. (c) A schematic describing an artificial photocatalytic H_2 production system using CdS NRs as the photosensitizer and Ni_2P as the cocatalyst. Reproduced with permission from ref. 125. Copyright 2015, The Royal Society of Chemistry.

Recently, several transition metal phosphides have been developed as electrocatalysts and found with excellent H_2 evolution reaction activities. More recently, transition metal phosphides have been utilized as highly efficient H_2-evolution cocatalysts to enhance the photocatalytic acitivity of CdX semiconductors.[124-129] The work by Cao *et al.* have shown that the combination of CdS nanorods as the photocatalyst with water-soluble Ni_2P nanoparticles (5-8 nm) as the cocatalyst Ni_2P could create a highly efficient, stable, nobel-metal-free photocatalytic system for H_2 generation.[124] Under the optimal conditions, this resulted photocatalytic system could achieve a TON and turnover frequency (TOF) of 26300 and 2110 h^{-1}, respectively, based on Ni_2P cocatalyst. Very recently, Du and co-workers have demonstrated an integrated nanostructure composed of CdS nanorods as the photocatalyst and Ni_2P nanoparticles as the cocatalyst for visible light-driven H_2 evolution.[125] In this case, crystalline Ni_2P nanoparticles were

tightly anchored onto the one-dimensional CdS nanorods via an easy solvothermal methanol, forming Ni_2P/CdS heterostructure (**Fig. 11a,b**). Under optimal conditions, the Ni_2P/CdS heterostructured photocatalyst could achieve a H_2 evolution rate up to ~1200 mmol $h^{-1}mg^{-1}$, giving a TON of ~3 270 000 and a TOF of 36 400 for Ni_2P in 90 h, respectively. The apparent QE was ~41% at 450 nm. The exceptional activity in this photocatalytic system was probably contributed to fast charge separation between the Ni_2P and the CdS nanorods(**Fig. 11c**). Based on this study, they further employed other transition metal phosphides, such as MoP,[126] CuP,[127] and Fe_2P,[128] as H_2-evolution cocatalysts combined with CdS semicodncutors for photocatalytic H_2 production.

3.3.4 Hydrogenase and artificial molecular cocatalysts

Hydrogenases, one of the rare families of organometallic biomolecules, are unique H_2-activation catalysts as they can efficiently catalyze the reversible reduction of protons to H_2. In recent years, many investigations have indicated that some natural hydrogenases could be utilized as efficient cocatalysts to combine with CdX photocatalysts for visible-light driven H_2 production (Table 2). For example, Brow *et al.* have investigated the integration of Clostridium acetobutylicum [FeFe]-hydrogenase I (CaI) with MPA-capped CdTe nanocrystals (MPA = 3-mercaptopropionic acid) for photocatalytic H_2 evolution under visible-light illumination.[131] In this case, CaI could form stable photocatalytic complexes with MPA-capped CdTe through the molecular assembly between them, which was mediated by electrostatic interactions, as showed in **Fig. 12a**. In these enzymatically active complexes, rapid intermolecular photogenerated electron transfer from CdTe to CaI, which acts as H_2-evolution cocatalyst, could be achieved, leading to efficient H_2 generation. Under optimal conditions, the CdTe–CaI complexes could achieve a single wavelength QE of 9% (λ = 532 nm) and an AM 1.5 efficiency of 1.8% in the presence of ascorbic acid.

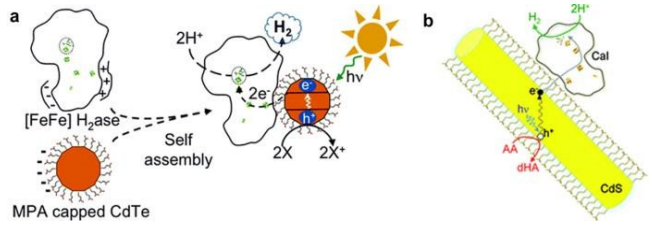

Fig. 12 (a) Schematic illustration of the self-assembly of CaI and MPA capped CdTe nanocrystals, and the light-induced H2 evolution of the self-assembled complex. (b) Schematic illustration of the photocatalytic H2 production by the CdS :CaI complex. (a) Reproduced with permission from ref. 131. Copyright 2010, American Chemical Society. (b)Reproduced with permission from ref. 132. Copyright 2012, American Chemical Society.

Based on this early work, Brown et al. recently further employed CaI as a cocatalyst combinaed with colloidal CdS nanorods, which possess a larger absorption cross-section and surface area compared to CdTe nanocrystals, for photochemical H_2 generation from water.[132] The resulted CdS nanorod-CaI photocatalytic complexes could display a TOF of 380–900 s^{-1} (based on hydrogenase) and a QE of up to 20% under illumination at 405 nm using ascorbic acid as a electro donor(see **Fig. 12b**). The advances in these investagations not only demonstrate the feasibility of the integration of natural hydrogenase cocatalysts with CdX photocatalysts for a sustainable and economically viable H_2 economy, but also provide some deeper insight into the rational design and preparation of other hybrid photocatalytic systems comprising of natural hydrogenases and inorganic semiconductors.

Despite hydrogenases are highly active for H_2 evolution, the poor stability and the high cost for separation and purification of the enzymes from natural systems limit their large scale application. Relatively speaking, biomimetic molecular complexes capable of mimicking the active sites of hydrogenases and reproducing the enzymic activity seem to be more promising, as they are more tolerant to O_2 and the structures are tunable. In recent years, many hybrid photocatalytic systems with CdX nanocrystals as photocatalysts and biomimetallic molecular complexes as coatalysts have been developed for photochemical H_2 generation. These hybrid systems were constructured either with molecular coatalysts and CdX photocatalysts as two separate components or with molecular catalysts covalently linked to the surface of CdX photocatalysts. This section mainly focuses on the development of the hybrid photocatalytic systems comprising CdX photocatalysts and Fe-,[133-137] Co-,[138-143] Ni-[144-147] and Cu-based[148] biomimetic complexes as molecular cocatalysts, with some representative examples summarized in Table 2.

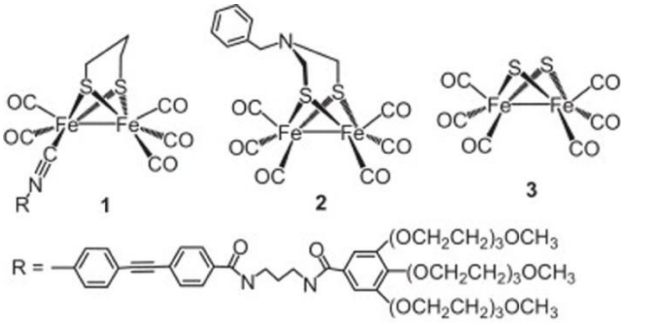

Fig. 13 Structures of [FeFe]-H_2ase mimics **1**-**3** used as cocatalysts in the hybrid systems with CdX nanocrystals. (**1**) Reproduced with permission from ref. 133. Copyright 2011, John Wiley and Sons. (**2**) Reproduced with permission from ref. 134. Copyright 2013, Nature Publishing Group. (**3**) Reproduced with permission from ref. 135. Copyright 2013, The Royal Society of Chemistry.

Since the structure of [FeFe] hydrogenase ([FeFe]-H_2ase) was resolved in 1998, many dinuclear [FeFe]-H_2ase mimics have been synthesized and employed as H_2 activation catalysts for both electrochemical and photochemical H_2 evolution. The first example of the incorporation of a [FeFe]-H_2ase mimics cocatalyst with CdX photocatalysts was reported in 2011 by Wu and coworkers.[133] In this study, a water soluble [FeFe]-H_2ase mimic (**1**, **Fig. 13**) containing a hydrophilic isocyanide ligand in combination with MPA-stabilized CdTe QDs and

ascorbate formed an efficient photocatalytic system for H_2 production in fully aqueous solutions at pH 4. The TON and TOF was up to 505 and 50 h^{-1} (based on **1**) after 10 h of illumination (λ> 400 nm). The researchers proposed that there existed a significant interaction between MPA-CdTe and **1** in the ground state and the oxidative quenching of the excited MPA-CdTe by **1** was the dominant pathway for the photocatalytic H_2 evolution. Studies on the similar hybrid system with $[Fe_2(CO)_6(\mu\text{-adt})CH_2C_6H_5]$ (**2**, **Fig. 13**) as molecular cocatalyst showed that the activity and stability of the [FeFe]-H_2ase mimic were significantly improved by addition of polysaccharide chitosanto mimic the protein matrix microenvironment surrounding the active site of [FeFe]-H_2ases.[134] The **2**/MPA-CdTe QD/H_2A system displayed a remarkable TON of 52,800 for photochemical H_2 evolutionin MeOH/H_2O at pH 4.5 in the presence of a large amount of chitosan (1.0 g L^{-1}) over 60 h of irradiation with 410 nm LEDs, affording an initial TOF of ~1.4 s^{-1} in the first 2 h. The TON of the H_2 evolu-tion and the stability of the system was significantly improved inthe presence of chitosan, which was attributed to the facts that (i) the encapsulation of MPA-CdTe QDs by polycationic chitosan prevented QDs from aggregating and enhanced the emission quantum efficiency of QDs and (ii) the intimate interaction of **2** and chitosan rendered the water insoluble catalyst well dispersed in aqueous solutions and improved the stability of the reduced species of **2**. These results demonstrated that not only the structure of the active center but also the biological environment surrounding the center in the natural [FeFe]-H_2ases should be taken into account when design and fabricate an active H_2 evolution systems based on [FeFe]-H_2ase mimics.

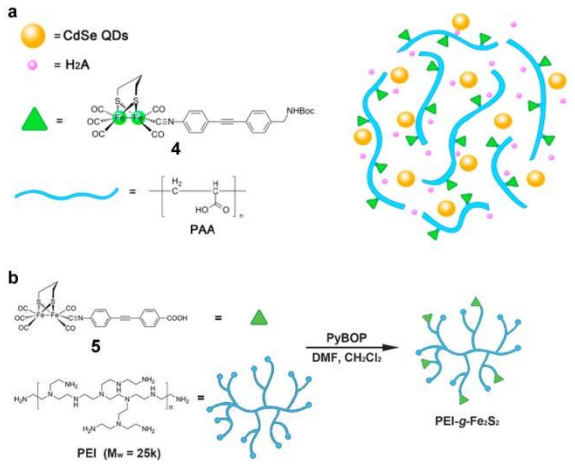

Fig. 14 (a) Proposed scaffold for the hybrid systems of PAA-**4**/MPA-CdSe QDs. (b) Schematic illustration of the synthetic route of PEI-g-Fe_2S_2 (**5**) production. (a) Reproduced with permission from ref. 136. Copyright 2013, John Wiley and Sons. (b) Reproduced with permission from ref. 137. Copyright 2015, John Wiley and Sons.

For most of [FeFe]-H_2ase mimics, their poor solubility in water is a critical drawback which limits their application for coupling with water splitting technology. In order to solve this problem, Wu and co-workers developed an effective strategy for interface-directed assembly of a simple [FeFe]-H_2ase mimic, $[Fe_2S_2(CO)_6]$ (**3**, **Fig. 13**),onto the surface of CdSe QDs, forming a water-soluble photocatalytic system for H_2 producton.[135] Under optimal conditions, the **3**/MPA-CdSe assembly system was able to reach a TON of 6530 based on **3** in water at pH 4.0 over 82 h of illumination with λ > 400 nm. A higher TON of 8781 was obtained when the same hybrid system was irradiated with 410 nm LEDs under otherwise identical conditions, giving a TOF of 596 h^{-1} in the first 4 h. The high efficiency and good durability of this system for photocatalytic H_2 production were ascribed to the close contact between the CdSe QDs and **3**. In addition to direct anchoring of the [FeFe]-H_2ase mimic to the QDs, the other strategy used by Wu and co-workers is to coanchor the [FeFe]-H_2ase mimic and the QDs to the side chain of a functionalized polymer.[136] In this case, both [FeFe]-H_2ase mimic **4** (**Fig. 14a**) and MPA-CdSe QDs were linked to the abundant carboxy groups in poly(acrylic acid) (PAA), leading to a short distance between the light harvester and the catalyst. PAA could enhance the emission of MPA-CdSe QDs and prevent MPA-CdSe nanoparticles from aggregating. The PAA-**4**/MPA-CdSe/H_2A system in water at an initial pH 4.0 displayed a TON of H_2evolution up to 27,135 over 8 h of irradiation with 450 nm LEDs, affording a TOF of 3.6 s^{-1} in the first half hour and a QE of 5.07%. Similarly, [FeFe]–H_2ase mimic **5** (see **Fig. 14b**) was anchored on branched polyethylenimone (PEI) to generate a water-soluble [FeFe]–H_2ase mimic, which then was coupled with MPA-capped CdSe QDs to create an efficient artificial photocatalytic system for H_2 evolution.[137]

Some molecular cobalt complexes are also employed to combine with CdX nanocrystals for photocatalytic H_2 production.[138-143] For example, by using CdS nanoparticles as the photocatalyst and cobaloxime complexes (**6**–**8**, **Fig. 15**) as molecular cocatalysts, Li and co-workers have demonstrated an efficient hybrid system for efficient photocatalytic H_2 evolution.[138] In this system, they found the physical adsorption of cobaloxime complexes on the surface of CdS particles facilitated the interfacial electron transfer from photoexcited CdS to cobaloxime complexes. Among various combinations of cobaloxime complexes with CdS, the cobaloxime **6**/CdS hybrid system showed the highest activity for H_2 production from a TEOA/H_2O/CH_3CN solution, giving a TON of 171 (based on **6**) for H_2 generation over 15 h of irradiation (λ > 420 nm) and a QE of 9.1% at 420 nm. In another example, a cobaloxime complex **9 (Fig. 15)** was anchored onto the surface of CdSe/ZnS core/shell QDs via a phosphonate linkage, generating a hybrid system.[139] In such a system, the ZnS shell could largely improve the photostability and fluorescence quantum efficiency of the QDs compared with CdSe without the shell. Consequently, the cobaloxime **9**/CdSe/ZnS system was capable of catalyzing H_2 generation photochemically in the presence of a proton source (triethylamine hydrochloride) and a sacrificial agent (TEOA) in toluene, giving a TON of over 10 000 H_2 per QD in 10 h. The work by Llobet et al. showed that the integration of a molecular cobalt cocatalyst **10** (**Fig. 15**) with CdTe QDs could result in efficient light-induced proton reduction to molecular H_2.[140] Chen et al. reported an efficient artificial photocatalytic system, consisting of CdS nanorods as

photocatalyst and Co-based complex **11 (Fig. 15)** as a molecular cocatalyst for H_2 generation.[141] Also, Sun and co-workers demonstrated a hybrid system with a coordinative interaction between a Co complex **12** (**Fig. 15**)and CdTe QDs displayed a high activity and improved stability for photochemical H_2 generation form water.[142]

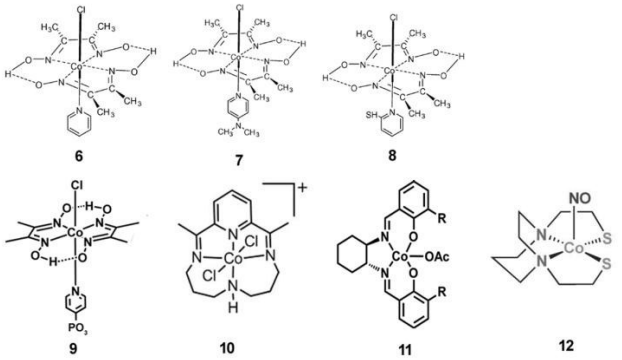

Fig. 15 Structures of Co-based complexes **6**-**12** used as cocatalysts in the hybrid systems with CdX nanocrystals. (**6**-**8**) Reproduced with permission from ref. 138. Copyright 2011, Elsevier. (**9**) Reproduced with permission from ref. 139. Copyright 2012, American Chemical Society. (**10**) Reproduced with permission from ref. 140. Copyright 2014, American Chemical Society. (**11**) Reproduced with permission from ref. 141. Copyright 2015, The Royal Society of Chemistry. (**12**) Reproduced with permission from ref. 142. Copyright 2015, The Royal Society of Chemistry.

In recent years, several molecular nickel complexes have been proved to be effective molecular cocatalysts in conjunction with CdX photocatalysts for photochemical H_2 evolution. In 2012, Krauss and coworkers showed that the integration of an *in situ* formed Ni-based complex, Ni^{2+}–DHLA (DHLA = dihydrolipoic acid) with DHLA-capped CdSe nanocrystals could create a highly active and superiorly stable hybrid system for visible-light-driven H_2 generation[144] (**see Fig. 16**). Upon irradiation of this catalytic system with 520 nm LEDs, a TON of more than 600 000 (based on Ni catalyst) and an initial TOF of 7000 h^{-1} was obtained in the presence of ascorbic acid as the electron donor, corresponding to a QE of over 36%. Moreover, this catalytic system presented undiminished activity for over 360 h. Very recently, by employing CdS nanosheets (~ 4 nm in thickness) as the photocatalyst and Ni-based complexes (**13–16**, see **Fig. 17**) as the molecular cocatalysts, our droup demonstrated an efficienf noble metal-free artificial photocatalytic system for H_2 production.[145] Among the CdS-complex systems containing various molecular nickel complexes (**13**-**16**), the CdS/complex **13** catalyst system exhibited the highest activity for H_2 production, which could generate H_2 with a TON of over 28 000 (based on complex **13**) in a TEA/CH_3OH/H_2O solution. We ascribed the high activity of this hybrid photocatalytic system to improvement in charge carrier separation and the efficient electron transfer from the CdS nanosheet to molecular nickel complexes. The work by Das et al. demonstrated Ni-based complexes (**17-21**, **Fig. 17**) for robust light-driven H_2 production from water in combination with CdSe QDs as photocatalyst.[146] Wang *et al*. reported the integration of Ni-DMSA complexes (DMSA = *meso*-2,3-dimercaptosuccinic acid) with DMSA capped CdSe/CdS core/shell nanocrystals for efficient photocatalytic H_2 production.[147]

Molecular copper complexes used for photochemical H_2 production in combination with CdX photocatalysts were less reported compared with iron, cobalt and nickel complexes. Zhang and co-workers showed a copper(I) cysteine complex formed by mixing Cu(II) ions with cysteine in aqueous solution could greatly enhance the activity of CdSe photocatalyst for H_2 evolution under visible light irradiation.[148] Differing from other molecular cocatalysts mentioned above, the copper(I) cysteine complex functioned as an oxidation cocatalyst, which could accepted the photogenerated holes from the VB of CdSe and complete its catalytic cycles with a high reaction rate. Under optimal conditions, the copper(I) cysteine complex could enhance the H_2 evolution rate by as much as 150 times.

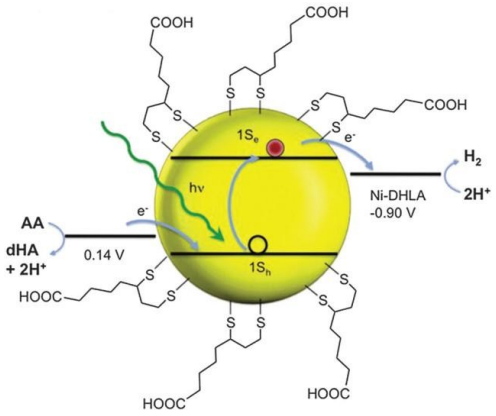

Fig. 16 Cartoon illustration of the relevant energies for H2 evolution (at pH 4.5). AA and dHA indicate ascorbic acid and dehydroascorbic acid, respectively. Reproduced with permission from ref. 144. Copyright 2012, The American Association for the Advancement of Science.

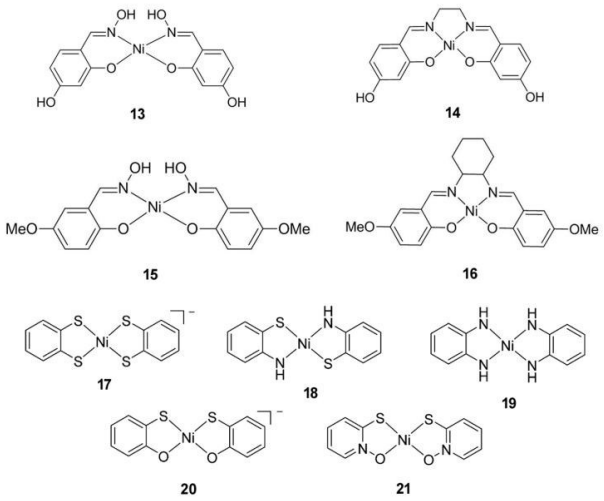

Fig. 17 Structures of Ni-based complexes **13**-**21** used as cocatalysts in the hybrid systems with CdX nanocrystals. (**13**-**16**) Reproduced with permission from ref. 145. Copyright 2015, John Wiley and Sons. (**17**-**21**) Reproduced with permission from ref. 146. Copyright 2015, American Chemical Society.

3.4 Hybridization of CdX with other semiconductors

3.4.1 Sensitization

Semiconductors with smaller bandgaps can be employed to sensitize those with larger bandgaps by forming semiconductor/semiconductor heterostructures. In the general sensitization mechanism, photogenerated electrons could be transferred from the CB of the smaller bandgap semiconductor to the CB of the larger bandgap semiconductor, leaving photogenerated holes in the VB of the smaller bandgap semiconductor.[14] Thus, photogenerated electrons and holes could be spatially separated from each other, leading to decreased recombination probability and increased electron lifetimes.

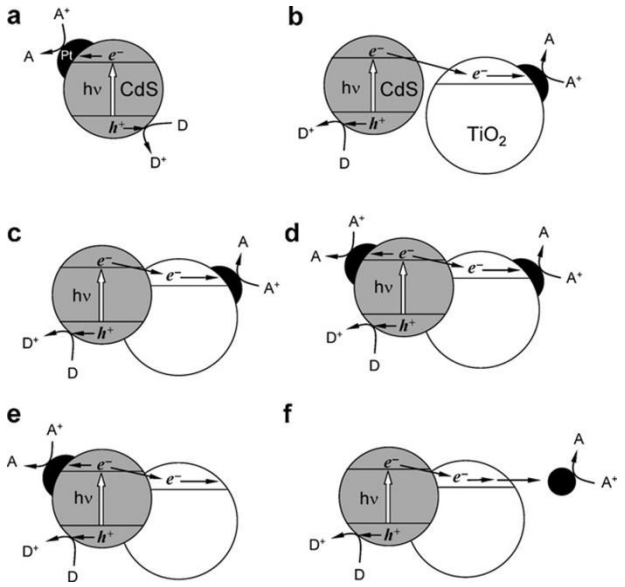

Fig. 18 Illustrative diagrams of the electron transfer in various hybrid photocatalysts comprised of CdS, TiO_2, and Pt. Reproduced with permission from ref. 157. Copyright 2008, The Royal Society of Chemistry.

The combination of CdX photocatalysts with another wider bandgap semiconductor to form heterogeneous photocatalysts is an effective avenue to improve their photoactivity. Among them, CdS/TiO_2 systems have gained the most extensive studies.[149-167] For example, Lee *et al.* combined CdS nanowires with TiO_2 nanoparticles and fabricated a CdS/TiO_2 heterogeneous photocatalyst.[149] They proved that these CdS/TiO_2 heterogeneous photocatalysts exhibited a significantly higher H_2 evolution rate than CdS nanowires alone under the same conditions. Park *et al.* synthesized a series of ternary hybrid composites composed of CdS, TiO_2 and Pt and systematically investigated the effects of varied combinations of the components on the photocatalytic activity for H_2 generation.[157] The authors found that the separation and transfer behaviours of photogenerated charge carrier were greatly affected by how the ternary hybrid composites were organized. For achieving high efficiency in charge carrier separation, the direct particle-to-particle contact between CdS and TiO_2 was required, which facilitate the photogenerated electron transfer from CdS to TiO_2. Moreover, the activity of the ternary hybrid photocatalysts was found to be extremely sensitive to the loading position of Pt on the CdS-TiO_2 composite. The [CdS-(Pt/TiO_2)] nanocomposite formed by photodeposition of Pt nanoparticles onto TiO_2, followed by the loading of CdS onto the Pt/TiO_2, showed the highest H_2 evolution rate (**Fig. 18c**).

3.4.2 p-n heterojunctions

The fabrication of semiconductor-semiconducto p–n heterojunction represents another effective strategy to improve the photocatalytic performance. In this case, both n- and p-type semiconductors can be excited to generate electron–hole pairs and photogenerated electron-hole pairs could be efficiently separated owning to the internal electric field with the direction from the n-type semiconductor to the p-type semiconductor.[14] The migration of electron and hole to different termini may also yield improvement to charge carrier separation, and thus enhancement in photocatalytic activity for hydrogen generation.

By means of a hydrothermal assisted ion-exchange route, Hou *et al.* have synthesized heterogeneous CdS@TaON with a core–shell structure.[168] In such a structure, both of n-typed CdS and p-typed TaON can be excited to generate electron-hole pairs under visible-light irradiation. The resulted CdS@TaON core–shell structure could generate p-n heterojunctions between the two semiconductors due to the CB position of CdS was more negative than that of TaON while the VB position of TaON was more positive than that of CdS. Consequently, the photogenerated electrons could transport from CdS to TaON while the holes transport from TaON to CdS. Study on their photocatalytic activity for H_2 evolution from an aqueous solution of Na_2S and Na_2SO_3 showed that the optimized (1wt%) CdS@TaON heterogeneous photocatalyst could achieve a H_2 production rate of 1.53 mmol $h^{-1}g^{-1}$ by loading 0.4 wt% Pt cocatalyst under visible-light illumination, which was much higher than those of TaON (0.045 mmol $h^{-1}g^{-1}$) and CdS (0.0675 mmol $h^{-1}g^{-1}$) under the same comditions. Further, they found that the rate of H_2 production can be raised to a higher value by coupling the CdS@TaON heterogeneous photocatalyst containing 0.4 wt% Pt with 1 wt% graphene, reaching 3.315 mmol $h^{-1}g^{-1}$ with a QE of 31% at 420 nm.

3.4.3 Z-scheme combination

Besides sensitization and p-n heterojunctions, Z-scheme combination of two semiconductors to form heterogeneous structures is another alternative strategy to enhance the photocatalytic performance. Differing from sensitization and p-n heterojunction, photogenerated electrons in Z-scheme combination would migrate to semiconductors with higher VB and recombine with photogenerated holes there.[169-171] As a result, the strongly reductive electrons stayed in semiconductors with higher CB and the strongly oxidative holes were kept in those with lower VB, which could keep electron-driven reduction reaction and hole-driven oxidation reaction occurring in different regions in a single heterogeneous structure and thus could improve the photocatalytic efficiency.

Several CdX-based heterogeneous photocatalysts based on Z-scheme combination have been exploited for the efficient photocatalytic H_2 production.[172-180] In a typical example, Tada *et al.* have successfully prepared an anisotropic CdS–Au–TiO_2

nanojunction, in which CdS, TiO_2 and the electron-transfer medium (Au) were all spatially fixed.[172] As illustrated in **Fig. 19**, small Au nanoparticles(~3.4 nm) were tightly anchored onto the antase TiO_2, while CdS was coated on Au nanoparticles, forming Au@CdS/TiO_2. In this three-component CdS-Au-TiO_2 nanojunction, photogenerated electrons could migrate from TiO_2 to Au and to CdS under UV-light irradiation. Consequently, these photoinduced electrons confined in CB of CdS could drive the reductive reaction, while photoinduced holes kept in VB of TiO_2 could function for the oxidation reaction. Moreover, this Z-scheme combination can also restrict the photocorrosion of CdS because photogenerated holes in CdS can be recombined with electrons from TiO_2 via the electron-transfer medium (Au). Consequently, this three-component photocatalyst system exhibited a high photocatalytic activity, far exceeding those of single- and two-component system. What is more, they found that the H_2 evolution rate can be further accelerated by selective deposition of appropriate amount of Pt onto the surface of catalyst. In a recent example, Cha and co-workers demonstrated enhanced H_2 production from a novel DNA-assembled Z-Scheme TiO_2-CdS photocatalyst system.[175] In this study, DNA was used to assemble Pt@CdS nanorods and TiO_2 nanoparticles into a well-organized Z-scheme photocatalyst system, which exhibited a significant improvement in H_2 production compared to either single photocatalyst or unassembled, dispered catalyst mixtures. The work by Zhang *et al.* demonstrated an efficient Z-scheme photocatalyst system consisting of CdS and WO_3 for visible-light driven H_2 produciton.[176]

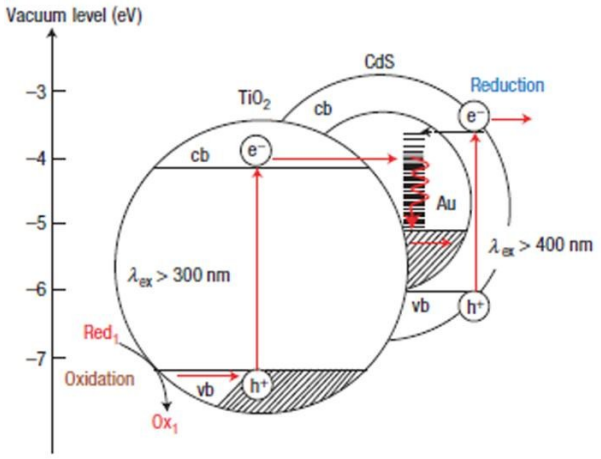

Fig. 19 Energy and diagram scheme of the CdS-Au-TiO_2 three-component systems. Reproduced with permission from ref.172. Copyright 2006, Nature Publishing Group.

3.5 Hybridization of CdX with carbon-based materials

Many carbon-related nano-structured materials such as carbon nanotubes (CNTs),[181-187] graphene or its derivatives,[97,103,114,188-202] and graphitic carbon nitride (g-C_3N_4)[203-209] are also widely used to stabilize and enhance the photoactivity of CdX semiconductors, as summarized in Table 3.

3.5.1 CdX/CNT heterogeneous photocatalysts

CNT, as a representative one-dimension structure allotrope of carbon, is usually used for hybriding with semiconductors for photocatalytic applications owing to their outstanding unique properties as follows[210-212]: (1) CNT possesses a large electron-storage capacity so that it can effectively accept photogenerated electrons from semiconductors in heterogeneous photocatalysts; (2) CNT can serve as excellent electron transporter and efficiently prevent the recombination of photogenerated carriers owing to its unique long-rang π electronic conjugation; (3) the high specific surface area of CNTs(>150 m^2 g^{-1}) could increase the adsorption of reactants; (4) CNT, as a semiconductor itself, might function as photoabsorbers to sensitize other ones.

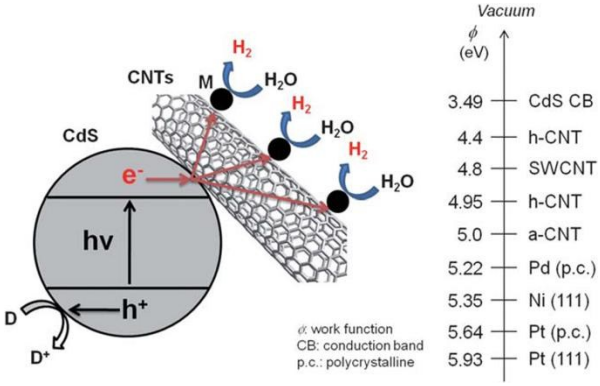

Fig. 20 Illustration of photocatalytic H_2production in CdS/CNT/M suspensions under light irradiation. M and D refer to metal catalyst and electron donor (Na_2S and Na_2SO_3), respectively. On the right-hand side, the reported work functions of selected materials are given. Reproduced with permission from ref.182. Copyright 2011, The Royal Society of Chemistry.

Peng *et al.* reported a hydrothermal method for the direct growth of CdS nanoparticles (12~28 nm) on surfaces of modified CNTs and successfully obtained CdS/CNT heterogeneous photocatalysts with different contents of CNTs.[181] In such a heterostructure, CdS nanoparticles were deposited on outer surfaces of CNTs, which resulting in an intimate contact between CdS nanoparticles and CNTs. The researchers demonstrated that those CdS/CNT heterogeneous photocatalysts with proper CNT contents exhibited much higher H_2 evolution rates than CdS alone. The optimal 10 wt% CdS–CNT photocatalyst system showed a H_2-evolution rate as high as 4.97 mmol h^{-1} g^{-1}, while the H_2 evolution rate over pure CdS nanoparticles was only 2.80 mmol h^{-1} g^{-1}. Moreover, they found that the presence of CNTs could enhance the stability of catalyst and suppress the photocorrosion of CdS. Kim and co-workers fabricated the ternary nanocomposites of CdS–CNT–M (M represents a transition metal) and studied their photocatalytic activity for H_2 production.[182] In this case, M was first deposited on CNTs, which were pretreated with acid, by means of chemical reduction with $NaBH_4$, followed by the loading of CdS nanoparticles on the as-obtained CNT/M, forming CdS/CNT/M three-component nanocomposites. The authors compared the activities of a series of CdS/CNT/M catalysts containing various M and demonstrated that the CdS/CNT/Pt system exhibited the highest rate of H_2 evolution (~0.825 mmol h^{-1} g^{-1}), which was obviously higher than that over CdS/CNT counterpart (**see Fig. 20**). The study by Yu and co-workers showed the H_2-evoltuion activity of $Cd_{0.1}Zn_{0.9}S$

photocatalyst could be improved by loading proper amount of CNTs. The optimal 0.25% CNT/ $Cd_{0.1}Zn_{0.9}S$ photocaalyst system could achieve a H_2-generation rate of 1.56 mmol h^{-1} g^{-1} with a QE of 7.9% at 420 nm.

3.5.2 CdX/graphene heterogeneous photocatalysts

Since it's first isolated in 2004 from graphite, graphene offers exciting new opportunities in various important fields, such as electronics and catalysis, owing to its two-dimensional structure with sp^2-bonded carbon atoms arranged in a honeycomb structure. Graphene possesses unique but excellent properties, such as rich surface chemistry, an extremely large surface area (~2620 m^2 g^{-1}), superior thermal and electrical conductivity, and great mechanical strength, which make it a good candidate to be bonded with semiconductors or to be used as supports for loading semiconductors for photocatalytic applications. The past several years have witnessed tremendous advances in the development of CdX semiconductor-graphene heterogeneous photocatalysts.[7,103,114,188-202] Generally, the key roles of grapheme in these CdX/grapheme photocatalyst systems including: (1) promoting photogenerated charge carrier separation and transfer; (2) inhibiting aggregation and overgrowth of CdX nanocrystals; (3) extending sunlight absorption range; (4) increasing the number of adsorption and active reaction sites.

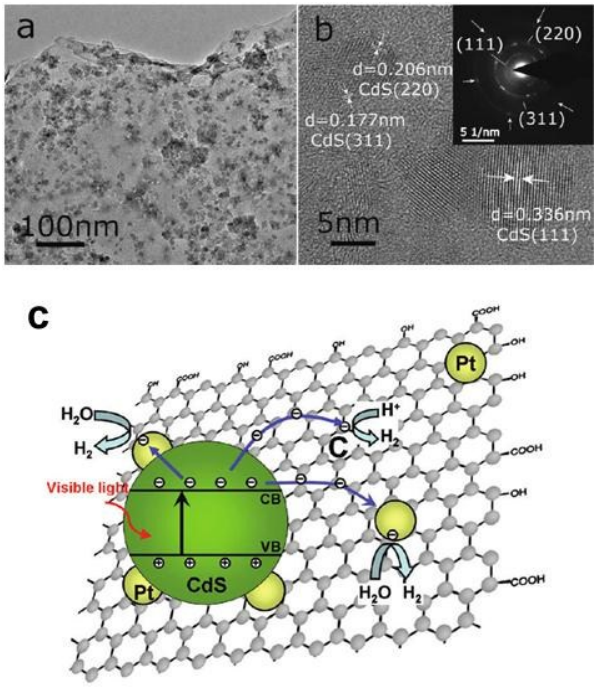

Fig. 21 (a) TEM and (b) HRTEM images of the graphene decorated with CdS clusters. The inset of (b) showed the SAED pattern. (c) Schematic illustration of the charge separation and transfer in the grahene-CdS photocatalyst system under visible light. Reproduced with permission from ref.188. Copyright 2011, American Chemical Society.

Gong, Yu and co-workers reported a highly-efficient CdS/graphene heterogeneous photocatalysts for photocatalytic H_2 production from water splitting under visible-light irradiation.[188] This CdS/graphene system was fabricated by means of a facile solvothermal method. The optimal CdS/grapheme (1.0 wt%) photocatalyst system could achieve a high H_2-production rate of 56 mmol $h^{-1}g^{-1}$ with loading of 0.5 wt% Pt cocatalyst (about 4.87 times higher than that of pure CdS nanoparticles), corresponding to an apparent QE of 22.5% at 420 nm. The authors demonstrated that graphene in the CdS/graphene system could serve as an electron collector and transporter to efficiently lengthen the lifetime of photogenerated charge carriers from CdS nanoparticles (see **Fig. 21**), which leading to enhanced photocatalytic activity for H_2 generation. The work by Zhang et al. showed that the nanocomposite photocatalyst consisting of reduced graphene oxide and $Zn_xCd_{1-x}S$ exhibited high activity for photocatalytic H_2 production.[197] Some modified graphene materials have also been incorporated with semiconductors to improve their photocatalytic properties.[198-200] In a typical example, Jia and co-workers coupled CdS with N-doped graphene to construct a highly-efficient photocatalyst system.[198] At an optimal content of N-graphene (2 wt%), the rate of H_2 production over CdS/N-graphene reached 1.05 mmol $h^{-1}g^{-1}$, while the H_2 evolution rates over CdS/graphene and pure CdS counterpart were only 0.495 mmol $h^{-1}g^{-1}$ and 0.2 mmol $h^{-1}g^{-1}$, respectively. They clarified that graphene doped with N could effectively alter the electron density of states in graphene and enhance the conductivity of graphene. Moreover, the N-graphene could act as a protective layer which effectively prevent CdS from photocorrosion under irradiation during photocatalytic process. Furthermore, Wang and co-workers compared the photocatalytic activity of CdS/graphene and CdS/CNT heterogeneous photocatalysts under the same conditions.[201] In this case, CdS nanoparticles (~ 35 nm) were loaded on graphene sheets or outer surfaces of CNTs, forming heterogeneous photocatalysts. They found the H_2-production rate over the optimal CdS/graphene system (0.7 mmol h^{-1} g^{-1}) was higher than that of the optimal CdS/CNT counterpart (0.52 mmol $h^{-1}g^{-1}$). Noticeably, both of the H_2-production rates over CdS/graphene and CdS/CNT systems were higher than that of single CdS photocatalyst (0.145 mmol $h^{-1}g^{-1}$). The researchers attributed the enhancement in photocatalytic activity over CdS/graphene photocatalyst system to the stronger interactions or the larger contact interface between CdS and graphene. These results demonstrated that by taking the advantages of carbon related materials in composites, the photocatalytic activity and stability of semiconductors can be remarkably improved.

3.5.3 CdX/g-C_3N_4 heterogeneous photocatalysts

Recently, g-C_3N_4 has shown promising applications in photocatalysis and photoelectrocatalysis due to its unique semiconducting properties and excellent chemical and thermal stability.[213] Many studies have demonstrated that it was a good candidate to be bonded with semiconductors or to be used as supports for loading semiconductors for constructing superior heterogeneous photocatalysts. For instance, Ge et al. prepared CdS QDs/g-C_3N_4 nanocomposites via a chemical impregnation method, which showed efficient activity for photocatalytic H_2 production.[203] The optimal loading content of CdS QD was found to be 30 wt %, and the corresponding visible-light-driven H_2 evolution rate from the resulted CdS/g-

C_3N_4 photocatalyst system reached 0.173 mmol $h^{-1}g^{-1}$ with 1.0 wt% Pt cocatalyst loading, exceeding that of Pt/g-C_3N_4 by more than 9 times. Similarly, Xue and co-workers reported the in-situ growth of CdS QDs on g-C_3N_4 nanosheets via a dimethyl sulfoxide (DMSO) involved solvothermal method.[204] The optimal CdS(12wt%)/g-C_3N_4 exhibited a 115 times higher H_2-evolution rate than of pure g-C_3N_4. In a recent example, Yu and co-workers synthesized CdS/g-C_3N_4 core/shell nanowires with different g-C_3N_4 contents by a combined solvothermal and chemisorptions method[205] (**Fig. 22a**). The optimal g-C_3N_4 content was determined to be 2 wt %. In this case, g-C_3N_4 could form thin and unclosed shells on CdS nanowires. In such CdS/g-C_3N_4 core/shell nanowires, the well-matched overlapping band structures between CdS and g-C_3N_4 facilitate the separation of photogenerated charge carriers(**Fig. 22b**). Consequently, this CdS/g-C_3N_4 photocatalyst system could reach a H_2-production rate up to 4.152 mmol $h^{-1}g^{-1}$ with an apparent QE up to 4.3% at 420 nm. Moreover, the resulted CdS/g-C_3N_4 photocatalyst system exhibited excellent photostability due to the corrosive photogenerated holes could be effectively transferred from CdS to g-C_3N_4.

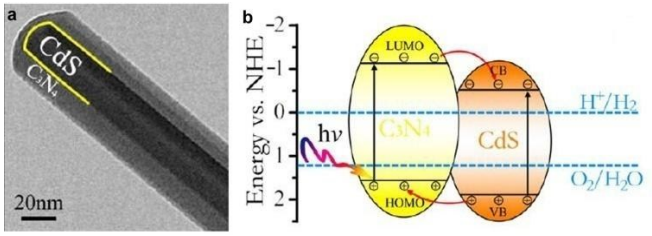

Fig. 22 (a) TEM image of the CdS/g-C_3N_4 core/shell nanowire. (b) Schematic illustration of the energy-level configuration and the photogenerated charge-transfer process between g-C_3N_4 and CdS. Reproduced with permission from ref.205. Copyright 2013, American Chemical Society.

4. Conclusions and future perspective

The last few decades have witnessed a sustained increase in research attention on semiconductor-based photocatalysis applications. In present review, we selectively summarized and analyzed the recent progress in photocatalytic water splitting for H_2 production mediated by CdX semiconductors. It is encouraging that the efficiencies of photocatalytic H_2 production with CdX-based photocatalysts have been tremendously improved benefitting from the great advances in material science and nanotechnology during past few decades.

Bulk CdX semicondcutors alone display low photoactivity and bad stability for H_2 production due to the ultrafast surface/bulk recombination of photogenerated charge carriers and the large H_2 evolution overpotential, while researchers have made great achievements in designing and synthesizing CdX materials, especially those in nanoscale size, with controlled size, shape, morphology, as well as crystal structure, to improve their photocatalytic performance. To further address the issues of low activity and bad stability in photocatalysis, current efforts are focused on the modification of CdX with other materials to enhance their photocatalytic activity and stability. Promising strategies such as forming solid solution, loading cocatalysts and hybridization with other semiconductors or carbon-based materials have been widely developed for CdX semiconductors to maximize the photoactivity. These strategies can significantly facilitate photogenerated electrons and holes separation and migration, reduce charge recombination probability, improve photoactivity and prolong functional life-time of photocatalysts.

Despite these progresses, several challenges still need to be addressed to obtain a satisfying H_2 production efficiency from solar water splitting. Firstly, the current state-of-the-art CdX-based photocatalyst systems is still far from being used for sustainable H_2 production from water with both economic and environmental benefit. Secondly, the photocorrosion of CdX under irradiation in photocatalytic process and the poor photostability are still key problems obstructing their large-scale application. Thirdly, for most of the CdX-based heterogeneous photocatalyst systems, the interrelationships among compositions, microstructures and photocatalytic performance are no clear and systematic answers. Additionally, introducing additional electron donors (sacrificial reagents) to achieve efficient H_2 production from water is needed in most of current photocatalytic systems.

In order to address these challenges and promote the further development of CdX-based photocatalytic H_2 production, further work in this field of should be focused on following aspects: (i) exploiting novel CdX-based photocatalysts with controlled structure, composition and morphology and tune their light absorption properties, bandgaps and the band-edge positions; (ii) conducting more in-depth theoretical and computational studies to probe into the interrelationships among compositions, microstructures and photocatalytic properties; (iii) developing more novel and effective modification strategies to enhance the photocatalytic activity and stability of CdX semicodncutors; (iv) exploring more new characterization technology to uncover the photogenerated charge carrier transfer dynamic and the mechanism of H_2 production in heterogeneous photosynthetic systems, which can purposefully direct the design and synthesis of highly efficient photocatalysts; (v) constructing highly-efficient photocatalytic systems to achieve overall water splitting from pure water without needing extra sacrificial reagents and organic solvents. Continued research in this exciting field will surely accelerate the development of photocatalytic water splitting technology and open new opportunities for expending other semiconductor-based photocatalytic applications, such as pollutant photodegradation, CO_2 photoreduction and organic photosynthesis.

Acknowledgements

We do appreciate the National Natural Science Foundation of China (No. 21422104) for financial support.

Notes and references

1 Y. Tachibana, L. Vayssieres and J. R. Durrant, *Nat. Photonics,* 2012, **6**, 511.
2 N. Armaroli and V. Balzani, *Angew. Chem. Int. Ed.,* 2007, **46**, 52.
3 J. Barber, *Chem. Soc. Rev.,* 2009, **38**, 185.
4 T. R. Cook, D. K. Dogutan, S. Y. Reece, Y. Surendranath, T. S. Teets, D. G. Nocera, *Chem. Rev.,* 2012, **110**, 6474.
5 J. Chow, R. J. Kopp, P. R. Portney, *Science*, 2003, **302**, 1528.
6 Z. Han, R. Eisenberg, *Acc. Chem. Res.,* 2014, **47**, 2537.
7 F. Wen and C. Li, *Acc. Chem. Res.,* 2013, **46**, 2355.
8 L.-Z. Wu, B. Chen, Z.-J. Li, C.-H. Tung, *Acc. Chem. Res.,* 2014, **47**, 2177.
9 A. Fujishima and K. Honda, *Nature*, 1972, **238**, 37.
10 M. B. Wilker, K. J. Schnitzenbaumer and G. Dukovic, *Isr. J. Chem.,* 2012, **52**, 1002.
11 M. Amelia, C. Lincheneau, S. Silvi and A. Credi, *Chem. Soc. Rev.,* 2012, **41**, 5728.
12 Q. Li, X. Li, S. W. Ahmed, A. Al-Ghamdi and J. Yu, *Adv. Energy Mater.,* 2015, **5**, 1500010.
13 X. Chen, S. Shen, L. Guo and S. S. Mao, *Chem. Rev.,* 2010, **110**, 6503.
14 W. Fan, Q. Zhang and Y. Wang, *Phys. Chem. Chem. Phys.*, 2013, **15**, 2632.
15 R. Marschall, *Adv. Funct. Mater.,* 2014, **24**, 2421.
16 A. Kudo and Y. Miseki, *Chem. Soc. Rev.,* 2009, **38**, 253.
17 J. Ran. J. Zhang, J. Yu, M. Jaroniec and S. Z. Qiao, *Chem. Soc. Rev.,* 2014, **43**, 7787.
18 Y. Xu and R. Xu, *Appl. Surf. Sci.,* 2015, **351**, 779.
19 X. Chen and W. Shangguan, *Front. Energy,* 2013, **7**, 111;
20 T. Hisatomi, J. Kubota and K. Domen, *Chem. Soc. Rve.,* 2014, **43**, 7520.
21 A. Vaneski, J. Schneider, A. S. Susha and A. L. Rogach, *J. Photoch. Photobio. C,* 2014, **19**, 52.
22 K. Zhang and L. Guo, *Catal. Sci. Technol.,* 2013, **3**, 1672.
23 F. E. Osterloh, *Chem. Soc. Rev.,* 2013, **42**, 2294.
24 C.-H. Liao, C.-W. Huang and J. C. S. Wu, *Catalysts*, 2012, **2**, 490.
25 M. Wang, K. Han, S. Zhang and L. Sun, Coord. *Chem. Rev.,* 2015, **287**, 1.
26 Y. Xu and B. Zhang, *Catal. Sci. Technol.,* 2015, **5**, 3084.
27 X. Li, J. Yu, J. Low, Y. Fang, J. Xiao and X. Chen, *J. Mater. Chem. A,* 2015, **3**, 2485.
28 Y. Qu and X. Duan, *Chem. Soc. Rve.,* 2013, **42**, 2568.
29 D. Zhang, G. Li, H. Li and Y. Lu, *Chem. Asian J.,* 2013, **8**, 26.
30 J. Yang, D. Wang, H. Han and C. Li, *Acc. Chem. Res.,* 2013, **46**, 1900.
31 D. Meisser, R. Memming and B. Kastening, *J. Phys. Chem.,* 1988, **92**, 3476.
32 N. Bao, L. Shen, T. Takata, K. Domen, A. Gupta, K. Yanagisawa, C. A. Grimes, *J. Phys. Chem. C,* 2007, **111**, 17527.
33 Y. Li, J. Du, S. Peng, D. Xie, G. Lu, S. Li, *Int. J. Hydrogen Energy,* 2008, **33**, 2007.
34 X. Wang, M. Liu, Z. Zhou and L. Guo, *J. Phys. Chem. C,* 2015, **119**, 20555.
35 J. Wang, B. Li, J. Chen, N. Li, J. Zheng, J. Zhao, Z. Zhu, *J. Alloy. Compd.,* 2012, **535**, 15.
36 F. A. Frame, E. C. Carroll, D. S. Larsen, M. Sarahan, N. D. Browning and F. E. Osterloh, *Chem. Commun.,* 2008, 2206.
37 Y. Xu, W. Zhao, R. Xu, Y. Shi and B. Zhang, *Chem. Commun.,* 2013, **49**, 9803.
38 Y. Huang, Y. Xu, J. Zhang, X. Yin, Y. Guo and B. Zhang, *J. Mater. Chem. A,* 2015, **3**, 19507.
39 Y. Peng, L. Shang, T. Bian, Y. Zhao, C. Zhou, H. Yu, L.-Z. Wu, C.-H. Tung and T. Zhang, *Chem. Commun.,* 2015, **51**, 4677.
40 M. Sathish and R. P. Viswanath, *Catal. Today* 2007, **29**, 421.
41 J. Zhao, M. A. Holmes and F. E. Osterloh, *ACS Nano,* 2013, **7**, 4316.
42 I. Grigioni, M. Bernareggi, G. Sinibaldi, M. V. Dozzi and E. Selli, *Appl. Catal. A-Gen.,* 2015,DOI: 10.1016/j.apcata.2015.09.021.
43 Y. Yu, J. Zhang, X. Wu, W. Zhao and B. Zhang, *Angew. Chem. Int. Ed.,* 2012, **51**, 897.
44 M. Liu, L. Wang, G. Lu, X. Yao and L. Guo, *Energy Environ. Sci.,* 2011, **4**, 1372.
45 G. J. Liu, Z. H. Zhou and L. J. Guo, *Chem. Phys. Lett.,* 2011, **509**, 43.
46 J. Zhang, Q. Xu, S. Z. Qiao and J. Yu, *ChemSusChem,* 2013, **6**, 2009.
47 X. H. Zhang, D. W. Jing and L. J. Guo, *Int. J. Hydrogen Energy,* 2010, **35**, 7051.
48 M. Kimi, L. Yuliati and M. Shamsuddin, *Int. J. Hydrogen Energy,* 2011, **36**, 9453.
49 Y.-G. Yu, G. Chen, L-X. Hao, Y.-S. Zhou, Y. Wang, J. Pei, J.-X. Sun and Z.-H. Han, *Chem. Commun.,* 2013, **49**, 10142.
50 J. Yu, J. Zhang and M. Jaroniec, *Green Chem.,* 2010, **12**, 1611.
51 S. N. Garaje, S. K. Apte, S. D. Naik, J. D. Ambekar, R. S. Sonawane, M. V. Kulkarni, A. Vinu and B. B. Kale, *Environ. Sci. Technol.,* 2013, **47**, 6664.
52 J. Yu, Q. Li, S. Liu and M. Jaroniec, *Chem. Eur. J.,* 2013, **19**, 2433.
53 A. Kubacka, M. Fernández-García and G. Colón, *Chem. Rev.,* 2012, **112**, 1555.
54 K. Ikeue, S. Shiiba and M. Machida, *Chem. Mater.,* 2010, **22**, 743.
55 B. B. Kale, J.-O. Baeg, S. N. Lee, H. Chang, S.-J. Moon and C. W. Lee, *Adv. Funct. Mater.,* 2006, **16**, 1349.
56 X. Wu, Y. Yu, Y. Liu, Y. Xu, C. Liu and B. Zhang, *Angew. Chem. Int. Ed.,* 2012, **51**, 3211.
57 Q. Li, H. Meng, P. Zhou, Y. Zheng, J. Wang, J. Yu and J Gong, *ACS Catal.,* 2013, **3**, 882.
58 G. Zhang, D. Monllor-Satoca and W. Choi, *Catal. Sci. Technol.,* 2013, **3**, 1790.
59 N. Bao, L. Shen, T. Takata and K. Domen, *Chem. Mater.,* 2008, **20**, 110.
60 L. Amirav and A. P. Alivisatos, *J. Phys. Chem. Lett.,* 2010, **1**, 1051.
61 H. Yan, J. Yang, G. Ma, G. Wu, X. Zong, Z. Lei, J. Shi and C. Li, *J. Catal.,* 2009, **266**, 165.
62 Y. Wang, Y. Wang and R. Xu, *J. Phys. Chem. C,* 2013, **117**, 783.
63 J. U. Bang, S. J. Lee, J. S. Jang, W. Choi and H. Song, *J. Phys. Chem. Lett.,* 2012, **3**, 3781.
64 J. Yu, Y. Yu and B. Cheng, *RSC Adv.,* 2012, **2**, 11829.
65 J. Jin, J. Yu, G. Liu and P. K. Wong, *J. Mater. Chem. A,* 2013, **1**, 10927.
66 Q. Xiang, B. Cheng and J. Yu, Appl. Catal., B, 2013, **138**, 299;
67 L. A. Silva, S. Y. Ryu, J. Choi, W. Choi and M. R. Hoffmann, *J. Phys. Chem. C,* 2008, **112**, 12069.
68 M. Sathish, B. Viswanathan and R. P. Viswanath, *Int. J. Hydrogen Energy,* 2006, **31**, 891.
69 B. Girginer, G. Galli, E. Chiellini and N. Bicak, *Int. J. Hydrogen Energy,* 2009, **34**, 1176.
70 Y. X. Li, Y. F. Hu, S. Q. Peng, G. X. Lu and S. B. Li, *J. Phys. Chem. C,* 2009, **113**, 9352.
71 J. S. Jang, U. A. Joshi and J. S. Lee, *J. Phys. Chem. C,* 2007, **111**, 13280.
72 D. W. Jing and L. J. Guo, *J. Phys. Chem. B,* 2006, **110**, 11139.
73 N. Z. Bao, L. M. Shen, T. Takata, D. L. Lu and K. Domen, *Chem. Lett.,* 2006, **35**, 318.
74 T.-T. Zhuang, Y. Liu, M. Sun, S.-L. Jiang, M.-W. Zhang, X.-C. Wang, Q. Zhang, J. Jiang and S.-H. Yu, *Angew. Chem. Int. Ed.,* 2015, **54**, 11495.
75 P. Tongying, F. Vietmeyer, D. Aleksiuk, G. J. Ferraudi, G. Krylova and M. Kuno, *Nanoscale,* 2014, **6**, 4117.

76 R. M. Navarro, F. del Valle and J. L. G. Fierro, *Int. J. Hydrogen Energy,* 2008, **33**, 4265.
77 S. Saha, G. Das, J. Thote and R. Banerjee, *J. Am. Chem. Soc.,* 2014, **136**, 14845.
78 J. Thote, H. B. Aiyappa, A. Deshpande, D. D. Díaz, S. Kurungot and R. Banerjee, *Chem. Eur. J.,* 2014, **20**, 15961.
79 Y. J. Zhang and L. Zhang, *Appl. Surf. Sci.,* 2009, **255**, 4863.
80 R. Sasikala, A. R. Shirole, V. Sudarsan, K. G. Girija, R. Rao, C. Sudakar and S. R. Bharadwaj, *J. Mater. Chem.,* 2011, **21**, 16566.
81 I. B. Rufus, B. Viswanathan, V. Ramakrishnan and J. C. Kuriacose, *J. Photochem. Photobiol., A,* 1995, **91**, 63.
82 I. B. Rufus, V. Ramakrishnan, B. Viswanathan and J. C. Kuriacose, *Langmuir*, 1990, **6**, 565.
83 H. Wang, W. Chen, J. Zhang, C. Huang and L. Mao, *Int. J. Hydrogen Energy,* 2015, **40**, 340.
84 T. Simon, N. Bouchonville, M. J. Berr, A.r Vaneski, A. Adrović, D. Volbers, R. Wyrwich, M. Döblinger, A. S. Susha, A. L. Rogach, F, Jäckel, J. K. Stolarczyk and J. Feldmann, *Nat. Mater.,* 2014, **13**, 1013.
85 S. Chen, X. Chen, Q. Jiang, J. Yuan, C. Lin and W. Shangguan, *Appl. Surf. Sci.,* 2014, **316**, 590.
86 M. Zhukovskyi, P. Tongying, H. Yashan, Y. Wang and M. Kuno, *ACS Catal.,* 2015, **5**, 6615.
87 S. Cao, C.-J. Wang, X.-J. Lv, Y. Chen and W.-F. Fu, *Appl. Catal. B: Environ.,* 2015, **162**, 381.
88 C.-T. Dinh, M.-H. Pham, F. Kleitz and T.-O. Do, *J. Mater. Chem. A,* 2013, **1**, 13308.
89 Z.-J. Li, X.-B. Li, J.-J. Wang, S. Yu, C.-B. Li, C.-H. Tung and L.-Z. Wu, *Energy Environ. Sci.,* 2013, **6**, 465.
90 Z. Khan, M. Khannam, N. Vinothkumar, M. De and M. Qureshi, *J. Mater. Chem.,* 2012, **22**, 12090.
91 X. P. Chen, W. Chen, P. B. Lin, Y. Yang, H. Y. Gao, J. Yuan, W. F. Shangguan, *Catal. Commun.,* 2013, **36**, 104.
92 X. Chen, W. Chen, H. Gao, Y. Yang and W. Shangguan, *Appl. Catal. B: Environ.,* 2014, **152**-**153**, 68.
93 Z. Yan, H. Wu, A. Han, X. Yu and P. Du, *Int. J. Hydrogen Energy,* 2014, **39**, 13353.
94 J. Yuan, J. Wen, Q. Gao, S. Chen. J. Li, X. Li and Y. Fang, *Dalton Trans.,* 2015, **44**, 1680.
95 Z. Shen, G. Chen, Y. Yu, Q. Wang, C. Zhou, L. Hao, Y. Li, L. He and R. Mu, *J. Mater. Chem.,* 2012, **22**, 19646.
96 J. Ran, J. Yu and M. Jaroniec, Green Chem., 2011, **13**, 2708.
97 Z. Yan, X. Yu, A. Han, P. Xu and P. Du, *J. Phys. Chem. C,* 2014, **118**, 22896.
98 J. Ran, J. Zhang, J. Yu and S. Z. Qiao, *ChemSusChem*, 2014, **7**, 3426.
99 L. J. Zhang, R. Zheng, S. Li, B. K. Liu, D. J. Wang, L. L. Wang and T. F. Xie, *ACS Appl. Mater. Interfaces,* 2014, **6**, 13406.
100 J. M. Lee, J. L. Gunjakar, Y. Ham, I. Y. Kim, K. Domen and S.-J. Hwang, *Chem. Eur. J.,* 2014, **20**, 17004.
101 65 X. Zong, H. Yang, G. Wu, G. Ma, F. Wen, L. Wang and C. Li, *J. Am. Chem. Soc.,* 2008, **130**, 7176.
102 D. Cao-Thang, P. Minh-Hao, F. Kleitz and D. Trong-On, *J. Mater. Chem. A,* 2013, **1**, 13308.
103 T. Jia, A. Kolpin, C. Ma, R. C.-T. Chan, W.-M. Kwok and S. C. E. Tsang, *Chem. Commun.,* 2014, **50**, 1185.
104 M. Nguyen, P. D. Tran, S. S. Pramana, R. L. Lee, S. K. Batabyal, N. Mathews, L. H. Wong and M. Graetzel, *Nanoscale*, 2013, **5**, 1479.
105 J. Zhang, Z. Zhu and X. Feng, *Chem. Eur. J.,* 2014, **20**, 10632.
106 Y. Lu, D. Wang, P. Yang, Y. Du and C. Lu, *Catal. Sci. Technol.,* 2014, **4**, 2650.
107 J. Xiong, Y. Liu, D. Wang, S. Liang, W. Wu and L. Wu, *J. Mater. Chem. A,* 2015, **3**, 12631.
108 R. Sasikala, A. P. Gaikwad, O. D. Jayakumar, K. G. Girija, R. Rao, A. K. Tyagi and S. R. Bharadwaj, *Colloids and Surfaces A: Physicochem. Eng. Aspects,* 2015, **481**, 485.
109 J. Chen, X.-J. Wu, L. Yin, B. Li, X. Hong, Z. Fan, B. Chen, C. Xue and H. Zhang, *Angew. Chem. Int. Ed.,* 2015, **54**, 1210.
110 X. Zong, J. Han, G. Ma, H. Yan, G. Wu and C. Li, *J. Phys. Chem. C,* 2011, **115**, 12202.
111 M. L. Tang, D. C. Grauer, B. Lassalle-Kaiser, V. K. Yachandra, L. Amirav, J. Yano, J. R. Long and A. P. Alivisatos, *Angew. Chem., Int. Ed.,* 2011, **50**, 10203.
112 W. Zhang, Y. Wang, Z. Wang, Z. Zhong and R. Xu, *Chem. Commun.,* 2010, **46**, 7631.
113 J. Zhang, S. Z. Qiao, L. Qi and J. Yu, *Phys. Chem. Chem. Phys.,* 2013, **15**, 12088.
114 J. Zhang, L. Qi, J. Ran, J. Yu and S. Z. Qiao, *Adv. Energy Mater.,* 2014, **4**, 1301925.
115 N. Li, B. Zhou, P. Guo, J. Zhou and D. Jing, *Int. J. Hydrogen Energy,* 2013, **38**, 11268.
116 S. Devi, P. Korake, S.N. Achary and N. M. Gupta, *Int. J. Hydrogen Energy,* 2014, **39**, 19424.
117 J. Wang, B. Li, J. Chen, N. Li, J. Zheng, J. Zhao and Z. Zhu, *Appl. Surf. Sci.,* 2012, **259**, 118.
118 Y.-P. Yuan, S.-W. Cao, L.-S. Yin, L. Xu and C. Xue, *Int. J. Hydrogen Energy,* 2013, **38**, 7218.
119 L. J. Zhang, T. F. Xie, D. J. Wang, S. Li, L. L. Wang, L. P. Chen and Y. C. Lu, *Int. J. Hydrogen Energy,* 2013, **38**, 11811.
120 J. Zhang, Q. L. Xu, S. Z. Qiao and J. G. Yu, *ChemSusChem*, 2013, **6**, 2009.
121 L. J. Zhang, T. F. Jiang, S. Li, Y. C. Lu, L. L. Wang, X. Q. Zhang, D. J. Wang and T. F. Xie, *Dalton Trans.,* 2013, **42**, 12998.
122 H. Liu, K. Zhang, D. Jing, G. Liu and L. Guo, *Int. J. Hydrogen Energy,* 2010, **35**, 7080.
123 U. Gupta, B. G. Rao, U. Maitra, B. E. Prasad and C. N. R. Rao, *Chem. Asian J.,* 2014, **9**, 1311.
124 S. Cao, Y. Chen, C. –J. Wang, P. He and W.-F. Fu, *Chem. Commun.,* 2014, **50**, 10427.
125 Z. Sun, H. Zheng, J. Li and P. Du, *Energy Environ. Sci.,* 2015, **8**, 2668.
126 Q. Yue, Y. Wan, Z. Sun, X. Wu, Y. Yuan and P. Du, *J. Mater. Chem. A,* 2015, **3**, 16941.
127 Z. Sun, Q. Yue, J. Li, J. Xu, H. Zheng and P. Du, J. Mater. Chem. A, 2015, **3**, 10243.
128 Z. Sun, H. Chen, Q. Huang and P. Du, Catal. Sci. Technol., 2015,**5**, 4964.
129 S. Cao, Y. Chen, C.-C. Hou, X.-J. Lv and W.-F. Fu, *J. Mater. Chem. A,* 2015, **3**, 6096.
130 J. S. Jang, D. J. Ham, N. Lakshminarasimhan, W. Y. Choi and J. S. Lee, *Appl. Catal. A-Gen.,* 2008, **346**, 149.
131 K. A. Brown, S. Dayal, X. Ai, G. Rumbles and P. W. King, *J. Am. Chem. Soc.,* 2010, **132**, 9672.
132 K. A. Brown, M. B. Wilker, M. Boehm, G. Dukovic and P. W. King, *J. Am. Chem. Soc.,* 2012, **134**, 5627.
133 F. Wang, W. G. Wang, X. J. Wang, H. Y. Wang, C. H. Tung and L. Z. Wu, *Angew. Chem., Int. Ed.,* 2011, **50**, 3193.
134 J.-X. Jian, Q. Liu, Z.-J. Li, F. Wang, X.-B. Li, C.-B. Li, B. Liu, Q.-Y. Meng, B. Chen, K. Feng, C.-H. Tung and L.-Z. Wu, *Nat. Commun.,* 2013, **4**, 2695.
135 C.-B. Li, Z.-J. Li, S. Yu, G.-X. Wang, F. Wang, Q.-Y. Meng, B. Chen, K. Feng, C.-H. Tung and L.-Z. Wu, *Energy Environ. Sci.,* 2013, **6**, 2597.
136 F. Wang, W.-J. Liang, J.-X. Jian, C.-B. Li, B. Chen, C.-H. Tung and L.-Z. Wu, *Angew. Chem., Int. Ed.,* 2013, **52**, 8134.
137 W.-J. Liang, F. Wang, M. Wen, J.-X. Jian, X.-Z. Wang, B. Chen, C.-H. Tung and L.-Z. Wu, *Chem. – Eur. J.,* 2015, **21**, 3187.
138 F. Y. Wen, J. H. Yang, X. Zong, B. J. Ma, D. G. Wang and C. Li, *J. Catal.,* 2011, **281**, 318.

139 J. Huang, K. L. Mulfort, P. Du and L. Chen, *J. Am. Chem. Soc.,* 2012, **134**, 16472.
140 C. Gimbert-Suriñach, J. Albero, T. Stoll, J. Fortage, M.-N. Collomb, A. Deronzier, E. Palomares and A. Llobet, *J. Am. Chem. Soc.,* 2014, **136**, 7655.
141 H. Chen, Z. Sun, S. Ye, D. Lu and P. Du, *J. Mater. Chem. A,* 2015, **3**, 15729.
142 K. Han, M. Wang, S. Zhang, S. Wu, Y. Yang and L. Sun, *Chem. Conmun.,* 2015, **51**, 7008.
143 A. Das, Z. Han, M.G. Haghighi and R. Eisenberg, *Proc. Natl. Acad. Sci. U. S. A.,* 2013, **110**, 16716.
144 Z. Han, F. Qiu, R. Eisenberg, P. L. Holland and T. D. Krauss, Science, 2012, **338**, 1321.
145 Y. Xu, X. Yin, Y. Huang, P. Du and B. Zhang, *Chem. – Eur. J.,* 2015, **21**, 4571.
146 A. Das, Z. Han, W. W. Brennessel, P. L. Holland and R. Eisenberg, *ACS Catal.,* 2015, **5**, 1397.
147 P. Wang, J. Zhang, H. He, X. Xu and Y. Jin, *Nanoscale*, 2015, **7**, 5767.
148 Y. Peng, L. Shang, Y. Cao, G. I. N. Waterhouse, C. Zhou, T. Bian, L.-Z. Wu, C.-H. Tung and T. Zhang, *Chem. Commun.,* 2015, **51**, 12556.
149 J. S. Jang, H. G. Kim, U. A. Joshi, J. W. Jang and J. S. Lee, *Int. J. Hydrogen Energy,* 2008, **53**, 5975.
150 H. Fujii, M. Ohtaki, K. Eguchi and H. Arai, *J. Mol. Catal. A: Chem.,* 1998, **129**, 61.
151 J. S. Jang, S. M. Ji, S. W. Bae, H. C. Son and J. S. Lee, *J. Photochem. Photobiol., A,* 2007, **188**, 112.
152 J. S. Jang, H. G. Kim, P. H. Borse and J. S. Lee, *Int. J. Hydrogen Energy,* 2007, **32**, 4786.
153 J. S. Jang, W. Li, S. H. Oh and J. S. Lee, *Chem. Phys. Lett.,* 2006, **425**, 278.
154 J. S. Jang, S. H. Choi, H. G. Kim and J. S. Lee, *J. Phys. Chem. C,* 2008, **112**, 17200.
155 Y. J. Zhang, W. Yan, Y. P. Wu and Z. H. Wang, *Mater. Lett.,* 2008, **62**, 3846.
156 C. L. Li, J. A. Yuan, B. Y. Han, L. Jiang and W. F. Shangguan, *Int. J. Hydrogen Energy,* 2010, **35**, 7073.
157 H. Park, W. Choi and M. R. Hoffmann, *J. Mater. Chem.,* 2008, **18**, 2379.
158 L. Qi, J. Yu and M. Jaroniec, *Phys. Chem. Chem. Phys.,* 2011, **13**, 8915.
159 V. M. Daskalaki, M. Antoniadou, G. L. Puma, D. I. Kondarides and P. Lianos, *Environ. Sci. Technol.,* 2010, **44**, 7200.
160 D. He, M. Chen, F. Teng, G. Li, H. Shi, J. Wang, M. Xu, T. Lu, X. Ji, Y. Lv and Y. Zhu, *Superlattice. Microst.,* 2012, **51**, 799;
161 S. K. Parayil, J. Baltrusaitis, C.-M. Wu and R. T. Koodali, *Int. J. Hydrogen Energy,* 2013, **38**, 2656.
162 X. Cui, G. Jiang, M. Zhu, Z. Zhao, L. Du, Y. Weng, C. Xu, D. Zhang, Q. Zhang, Y. Wei, A. Duan, J. Liu and J. Gao, *Int. J. Hydrogen Energy,* 2013, **38**, 9065.
163 M. Khatamian, M. S. Oskoui, M. Haghighi and M. Darbandi, *Int. J. Energy Res.,* 2014, **38**, 1712.
164 J. Fang, L. Xu, Z. Zhang, Y. Yuan, S. Cao, Z. Wang, L. Yin, Y. Liao and C. Xue, *ACS Appl. Mater. Interfaces,* 2013, **5**, 8088;
165 H. N. Kim, T. W. Kim, I. Y. Kim and S. Hwang, *Adv. Funct. Mater.,* 2011, **21**, 3111.
166 D. Jing and L. Guo, *J. Phys. Chem. C,* 2007, **111**, 13437.
167 S. Qian, C. Wang, W. Liu, Y. Zhu, W. Yao and X. Lu, *J. Mater. Chem.,* 2011, **21**, 4945.
168 J. Hou, Z. Wang, W. Kan, S. Jiao, H. Zhu and R. V. Kumar, *J. Mater. Chem.,* 2012, **22**, 7291.
169 Y.-P. Yuan, L.-W. Ruan, J. Barber, S. C. J. Loo and C. Xue, *Energy Environ. Sci.,* 2014, **7**, 3934.
170 K. Maeda, *ACS Catal.,* 2013, **3**, 1486.
171 P. Zhou, J. Yu and M. Jaroniec, *Adv. Mater.,* 2014, **26**, 4920.
172 H. Tada, T. Mitsui, T. Kiyonaga, T. Akita and K. Tanaka, *Nat. Mater.,* 2006, **5**, 782.
173 L. Ding, H. Zhou, S. Lou, J. Ding, D. Zhang, H. Zhu and T. Fan, *Int. J. Hydrogen Energy,* 2013, **38**, 8244.
174 H. Zhu, B. Yang, J. Xu, Z. Fu, M. Wen, T. Guo, S. Fu, J. Zuo and S. Zhang, *Appl. Catal. B: Environ.,* 2009, **90**, 463.
175 K. Ma, O. Yehezkeli, D. W. Domaille, H. H. Funke and J. N. Cha, *Angew. Chem. Int. Ed.,* 2015, **54**, 11490.
176 L. J. Zhang, S. Li, B. K. Liu, D. J. Wang and T. F. Xie, *ACS Catal.,* 2014, **4**, 3724.
177 X. Wang, G. Liu, Z. Chen, F. Li, L. Wang, G. Lu and H. Cheng, *Chem. Commun.,* 2009, 3452.
178 X. Wang, G. Liu, L. Wang, Z.-G. Chen, G. Q. Lu and H.-M. Cheng, *Adv. Energy Mater.,* 2012, **2**, 42.
179 H. J. Yun , H. Lee , N. D. Kim , D. M. Lee , S. Yu and J. Yi , *ACS Nano,* 2011 , **5** , 4084.
180 Z. B. Yu , Y. P. Xie , G. Liu , G. Q. Lu , X. L. Ma , H. M. Cheng , *J. Mater. Chem. A,* 2013, **1** , 2773.
181 T. Peng, P. Zeng, D. Ke, X. Liu and X. Zhang, *Energy Fuels,* 2011, **25**, 2203.
182 Y. Kim and H. Park, *Energy Environ. Sci.,* 2011, **4**, 685.
183 J. G. Yu, B. Yang and B. Cheng, Nanoscale, 2012, **4**, 2670.
184 L. Wang, Z. Yao, F. Jia, B. Chen and Z. Jiang, *Dalton Trans.,* 2013, **42**, 9976.
185 G. Khan, S. K. Choi, S. Kim, S. K. Lim, J. S. Jang and H. Park, *Appl. Catal. B: Environ.,* 2013, **142**-**143**, 647.
186 X. Wang, M. Liu, Q. Chen, K. Zhang, J. Chen, M. Wang, P. Guo and L. Guo, *Int. J. Hydrogen Energy,* 2013, **38**, 13091.
187 Z. Yao, L. Wang, Y. Zhang, Z. Yu and Z. Jiang, *Int. J. Hydrogen Energy,* 2014, **39**, 15380.
188 Q. Li, B. Guo, J. Yu, J. Ran, B. Zhang, H. Yan and J. R. Gong, *J. Am. Chem. Soc.,* 2011, **133**, 10878.
189 T. Y. Peng , K. Li , P. Zeng , Q. G. Zhang and X. G. Zhang , *J. Phys. Chem. C,* 2012, **116** , 22720.
190 P. Zeng , Q. G. Zhang , T. Y. Peng and X. H. Zhang , *Phys. Chem. Chem. Phys.,* 2011 , **13** , 21496.
191 A. H. Ye , W. Q. Fan , Q. H. Zhang , W. P. Deng , Y. Wang , *Catal. Sci. Technol.,* 2012, **2**, 969.
192 K. Chang , Z. W. Mei , T. Wang , Q. Kang , S. X. Ouyang , J. H. Ye , *ACS Nano,* 2014, **8**, 7078.
193 Z. Khan , T. R. Chetia , A. K. Vardhaman , D. Barpuzary , C. V. Sastri , M. Qureshi , *RSC Adv.,* 2012, **2**, 12122.
194 X. W. Wang , L. C. Yin , G. Liu , *Chem. Commun.,* 2014, **50**, 3460 .
195 J. G. Hou , Z. Wang , W. B. Kan , S. Q. Jiao , H. M. Zhu , R. V. Kumar , *J. Mater. Chem.,* 2012, **22**, 7291.
196 J. G. Hou , C. Yang , H. J. Cheng , Z. Wang , S. Q. Jiao , H. M. Zhu, *Phys. Chem. Chem. Phys.,* 2013 , **15** , 15660 .
197 J. Zhang, J. G. Yu, M. Jaroniec and J. R. Gong, *Nano Lett.,* 2012, **12**, 4584.
198 L. Jia, D. Wang, Y. Huang, A. Xu and H. Yu, *J. Phys. Chem. C,* 2011, **115**, 11466.
199 X. J. Lv , W. F. Fu , H. X. Chang , H. Zhang , J. S. Cheng , G. J. Zhang , Y. Song , C. Y. Hu , J. H. Li , *J. Mater. Chem.,* 2012, **22**, 1539.
200 S. S. Zhang, H. J. Wang, M. S. Yeung, Y. P. Fang, H. Yu and F. Peng, *Int. J. Hydrogen Energy,* 2013, **38**, 7241.
201 A. Ye, W. Fan, Q. Zhang, W. Deng and Y. Wang, *Catal. Sci. Technol.,* 2012, **2**, 969.
202 Y. Hong, P. Shi, P. Wang and W. Yao, *Int. J. Hydrogen Energy,* 2015, **40**, 7045.
203 L. Ge, F. Zuo, J. Liu, Q. Ma, C. Wang, D. Sun, L. Bartels and P. Feng, *J. Phys. Chem. C,* 2012, **116**, 13708.
204 S.-W. Cao, Y.-P. Yuan, J. Fang, M. M. Shahjamali, F. Y. C. Boey, J. Barber, S. C. J. Loo and C. Xue, *Int. J. Hydrogen Energy,* 2013, **38**,1258.
205 J. Zhang, Y. Wang, J. Jin, J. Zhang, Z. Lin, F. Huang and J. Yu, A*CS Appl. Mater. Interfaces,* 2013, **5**, 10317.

206 W. Li, C. Feng, S. Dai, J. Yue, F. Hua and H. Hou, *Appl. Catal. B: Environ.,* 2015, **168**-**169**, 465.
207 F. Jiang, T. Yan, H. Chen, A. Sun, C. Xu and X. Wang, *Appl. Surf. Sci.,* 2014, **295**, 164.
208 H. Yu, F. Chen, F. Chen and X. Wang, *Appl. Surf. Sci.,* 2015, **358**, 385.
209 J. Yuan, J. Wen, Y. Zhong, X. Li, Y. Fang, S. Zhang and W. Liu, *J. Mater. Chem. A.,* 2015, **3**, 18244.
210 L. Wang, H. Liu, R. M. Konik, J. A. Misewich and S. S. Wong, *Chem. Soc. Rve.,* 2013, **42**, 8134.
211 Y. Yan, J. Miao, Z. Yang, F.-X. Xiao, H. B. Yang, B. Liu and Y. Yang, *Chem. Soc. Rev.,* 2015, **44**, 3295.
212 Z. Yang, J. Ren, Z. Zhang, X. Chen, G. Guan, L. Qin, Y. Zhang and H. Peng, *Chem. Rev.,* 2015, **115**, 5159.
213 S. Cao and J. Yu, *J. Phys. Chem. Lett.,* 2014, **5**, 2101.

Table 1 CdX-based photocatalysts containing inorganic cocatalysts for photocatalytic H_2 production.

Photocatalyst	Cocatalyst	Light source[a]	Aqueous reaction solution[b]	H_2 evolution			Ref.
				Activity ($\mu molh^{-1}g^{-1}$)	QE (%)	Enhancement Factor[c]	
Nanoporous CdS nanostructures	13wt% Pt	λ ≥ 420 nm (Xe)	0.35 M Na_2SO_3 + 0.25 M Na_2S	27333	60.34(420 nm)	205	59
CdSe-seeded CdS nanorods	Pt	300 W Xe	Isopropanol	40000	20 (450 nm)		60
CdS	0.3 wt% Pt + 0.13 wt% PdS	λ > 420 nm (Xe)	0.5 M Na_2SO_3 + 0.5 M Na_2S	29233	93 (420 nm)	381	61
CdS	1 wt% Pt	λ > 420 nm (Xe)	0.1 M Na_2SO_3 + 0.1 M Na_2S	13800	22 (420 nm)		62
CdSe nanorods	Pt	λ ≥ 420 nm (Xe)	0.35 M Na_2SO_3 + 0.25 M Na_2S	36250	0.63 (454 nm)		63
Multi-armed CdS nanorods	0.23 wt% Pt	λ ≥ 420 nm (Xe)	10 v% lactic acid	24200	51 (420 nm)	60.5	64
Single crystal CdS nanowires	0.3 wt% Pt	λ ≥ 420 nm (Xe)	10 v% lactic acid	18625	61.7 (420 nm)	74.5	65
Porous CdS nanosheet-based flowers	0.5 wt% Pt	λ > 420 nm (Xe)	10 v% lactic acid	9374	24.7 (420 nm)		66
Mixed-phase CdS	0.3 wt% Pt	λ > 400 nm (Hg-Xe)	0.02 M Na_2SO_3 + 0.1 M Na_2S	668		2	67
CdS	1 wt% Pt	UV	0.35 M Na_2SO_3 + 0.24 M Na_2S	6000		8.82	68
CdS	1 wt% Pt	Overall spectrum	0.3 M Na_2SO_3 + 0.2 M Na_2S	13860	1.3 (overall spectrum)	3.3	69
CdS nanorods	0.05 wt% Pt	λ >420 nm (Hg)	Formic acid	4603.2	13.9 (>420 nm)	21	70
CdS	1.5 wt% Pt	λ >420 nm (Hg)	Formic acid	1127.5		16.3	33
CdS nanowires	1 wt% Pt	λ ≥ 420 nm (Hg)	0.1 M Na_2S + 0.02 M Na_2SO_3	~60			71
CdS	3 wt% Pt	λ ≥ 420 nm (Hg)	0.25 M Na_2S + 0.35 M Na_2SO_3	83.3			32
CdS	2 wt% Pt	λ > 430 nm (Xe)	0.25 M Na_2SO_3 + 0.35 M Na_2S	5625	24.1 (420 nm)	5	72
CdS nanowire arrays	10 wt% Pt	λ ≥ 420 nm (Xe)	0.25 M Na_2SO_3 + 0.35 M Na_2S	2600	7.2 (420 nm)		73
CdS	1 wt% Pt	UV	0.35 M Na_2SO_3 + 0.24 M Na_2S	14150		19.4	40
ZnS-CdS heteronanorods	Pt	300 W Xe	0.25 M Na_2SO_3 + 0.35 M Na_2S	5050		7.5	74
CdSe/CdS core/shell nanowires	~30wt% Pt	450 W Xe	0.1 M Na_2SO_3 + 0.1 M Na_2S	434.29		5.4	75
CdS-ZnO-CdO	0.5 wt% Ru	150 W Xe	0.1 M Na_2S + 0.04 M Na_2SO_3	~75		50	76
CdS/Al-HMS	0.07 wt% Ru	λ ≥ 420 nm (Xe)	Formic acid	825.9	1.2 (420 nm)		79
CdS	4 wt% Ni	λ > 420 nm (Xe)	$(NH_4)_2SO_3$	25848	26.8 (420 nm)		83
CdS nanorods	Ni	447 nm (LED)	Ethanol	63000	53 (447 nm)		84
CdS	5 wt% Ni	λ > 400 nm (Xe)	50 v% lactic acid	30048		~6.6	85
CdS-titanate	1.2 wt% Ni	λ ≥ 420 nm (Xe)	20 v% Ethanol	11038	21 (420 nm)	77.7	88
CdS	32 mol% NiO	500W phoenix tungsten halogen lamp	0.25 M Na_2SO_3 + 0.35 M Na_2S	745	6.02		90
CdS	13.2 mol% Ni_2O_3	λ > 400 nm (Xe)	30 v% Methanol	4456		4.1	91
CdS	1 mol % NiO_x	λ > 400 nm (Xe)	30 v% Methanol	5908	8.6 (400 nm)	117	92
TiO_2/CdS	2.1 wt% CoO_x	λ > 400 nm (Xe)	0.125 M Na_2S + 0.175M Na_2SO_3	660		7	93
CdS	3 mol% Co_3O_4	λ ≥ 420 nm (Xe)	0.5 M Na_2S + 0.5M Na_2SO_3	236		32.4	94
CdS	3.5 mol% MoO_3	λ > 400 nm (Xe)	0.2 M Na_2S + 1.5M Na_2SO_3	5250	28.86 (420 nm)	87.5	95
CdS	23 mol% $Ni(OH)_2$	λ > 420 nm (Xe)	25 v% TEOA	5085	28 (420 nm)	145	96
CdS/RGO	1.0 wt% $Ni(OH)_2$	λ > 420 nm (Xe)	0.25 M Na_2SO_3 + 0.35 M Na_2S	4731		10	97

$Zn_{0.8}Cd_{0.2}S$	0.6 mol% $Ni(OH)_2$	λ ≥ 420 nm (Xe)	20 v% TEOA	7160	29.5 (420nm)	25.5	98
CdS nanorods	6.8 mol% $Co(OH)_2$	500 W Xe	25 v% Methanol	61		41	99
CdS	0.2 wt% MoS_2	λ > 420 nm (Xe)	10 v% lactic acid	~5400		36	101
CdSe	0.5 wt % MoS_2	λ ≥ 420 nm (Xe)	0.1 M Na_2SO_3 + 0.1 M Na_2S	890		3.7	102
CdS	0.4 wt% RGO + 2 wt% MoS_2	500 W UV lamp	10 v% lactic acid	6857		71	103
$Zn_{0.2}Cd_{0.8}S$	3 wt% MoS_2	λ > 420 nm (Xe)	0.25 M Na_2SO_3 + 0.35 M Na_2S	420		210	104
$Zn_{0.3}Cd_{0.7}S$	0.6 wt% MoS_2	λ > 420 nm (Xe)	10 v% lactic acid	1196		7	106
CdS	15 wt% MoS_2	λ > 420 nm (Xe)	0.02 M Na_2SO_3 + 0.1 M Na_2S	4770		10	107
CdS	~11 mol% WS_2	λ > 420 nm (Xe)	10 v% lactic acid	1984		16	109
	~7 mol% MoS_2	λ > 420 nm (Xe)	10 v% lactic acid	1472		12	109
CdS	1.0 wt% WS_2	λ > 420 nm (Xe)	10 v% lactic acid	~4200	5.0 (420 nm)	28	110
CdSe/CdS	MoS_3	450 nm (Hg-Xe)	TEOA	100000	10 (450 nm)		111
CdS	1.2 mol% NiS	λ ≥ 420 nm (Xe)	30vol% lactic acid	7267	51.3 (420 nm)	34	112
CdS nanorods	5 mol% NiS	λ> 420 nm (Xe)	0.25 M Na_2SO_3 + 0.35 M Na_2S	1131	6.1 (420nm)	20.6	113
$Zn_{0.5}Cd_{0.5}S$/RGO	3 mol% NiS	AM1.5	0.25 M Na_2SO_3 + 0.35 M Na_2S	7514	31.3 (420nm)	1.8	114
$Cd_{0.5}Zn_{0.5}S$	0.025 mol% NiS	λ ≥ 430 nm (Xe)	0.25 M Na_2SO_3 + 0.35 M Na_2S	1400	33.9 (425nm)	3.5	115
$CdLa_2S_4$	2 wt% NiS_2	λ ≥ 420 nm (Xe)	0.25 M Na_2SO_3 + 0.35 M Na_2S	2500	1.6 (420nm)	3.1	118
CdS nanorods	3 mol% CuS	500 W (Xe)	0.25 M Na_2SO_3 + 0.35 M Na_2S	332		3.5	119
$Zn_{0.5}Cd_{0.5}S$	CuS	λ ≥ 420 nm (Xe)	0.25 M Na_2SO_3 + 0.35 M Na_2S	4638.5	20.9 (420nm)	7	120
$Zn_{0.8}Cd_{0.2}S$	3 wt% CuS	500 W (Xe)	0.25 M Na_2SO_3 + 0.35 M Na_2S	2792	36.7 (420nm)	4.4	121
CdS	20 mol% SrS	λ ≥ 430 nm (Xe)	0.25 M Na_2SO_3 + 0.35 M Na_2S	615	2.85 (420 nm)	2	122
CdS	~41.6mol% TiS_2	λ> 399 nm (Xe)	3.5v% Benzyl alcohol	1000		2.9	123
CdS	~41.6mol%TaS_2	λ> 399 nm (Xe)	3.5v% Benzyl alcohol	2320		6.9	123
CdS nanorods	0.5 wt% Ni_2P	λ> 420 nm (Xe)	0.25 M Na_2SO_3 + 0.35 M Na_2S	1200000	41(450 nm)	22	125
CdS nanorods	16.7 wt% MoP	λ> 420 nm (Xe)	10 v% lactic acid	163200	5.8(450 nm)	9.2	126
CdS nanorods	0.44 wt% Cu_3P	λ> 420 nm (Xe)	1.25 M Na_2S + 1.75 M Na_2SO_3	200000	25(450 nm)	6.6	127
CdS nanorods	30 wt% Fe_2P	λ> 420 nm (Xe)	0.5 M AA	186000	15(450 nm)	31	128
CdS	10wt% WC	λ≥ 420 nm (Hg-arc)	0.1 M Na_2S + 0.02 M Na_2SO_3	1400		23	130

[a] Xe: xenon lamp, Hg: mercury lamp. [b] TEOA: triethanolamine, AA: ascorbic acid.
[c] Enhanced factor is calculated from the activity enhancement of photocatalysts loaded with the optimal amount of cocatalysts over photocatalysts without the loading of cocatalysts.

Table 2 CdX-based photocatalysts containing hydrogenase and molecular cocatalysts for photocatalytic H_2 production.

Photocatalyst	Cocatalyst[a]	Light source[b]	Solvent	Sacrificial reagent[c]	H_2 evolution			Ref.
					TON vs. cocatalyst	TOF vs. cocatalyst	QE (%)	
CdTe	CaI	AM 3.0 (TH)	H_2O	AA		25 s^{-1}	9 (532 nm)	131
CdS	CaI	405 nm (LED)	H_2O	AA	~1000000	380 s^{-1}	20 (405 nm)	132
		AM 1.5 (LED)	H_2O	AA		983 s^{-1}		
CdTe	**1**	λ> 400 nm (Hg)	H_2O	AA	505	50 h^{-1}		133
CdTe	**2** + chitosan	410 nm (LED)	CH_2OH/H_2O	AA	52800	~1.4 s^{-1}		134
CdSe	**3**	410 nm (LED)	H_2O	AA	8781	596 h^{-1}		135
CdSe	**4** + PAA	450 nm (LED)	H_2O	AA	27135	3.6^{-1}	5.07 (450 nm)	136
CdSe	**5** + PEI	410 nm (LED)	H_2O	AA	10600			137
CdS	**6**	λ> 420 nm (Xe)	CH_3CN/H_2O	TEOA	171		9.1(420 nm)	138
CdSe/ZnS	**9**	λ> 400 nm (Xe)	toluene	TEOA	>151			139
CdTe	**10**	λ> 400 nm (Xe)	H_2O	AA	650	9 min^{-1}		140
CdS	**11**	λ> 420 nm (Xe)	H_2O	Na_2SO_3 + Na_2S	64700		29 (420 nm)	141
CdTe	**12**	λ> 400 nm (Xe)	H_2O	AA	14400	850 h^{-1}	5.32(400 nm)	142
CdSe	Ni^{2+}-DHLA	520 nm (LED)	H_2O	AA	>600000	7000 h^{-1}	36 (520 nm)	144
CdS	**13**	λ> 420 nm (Xe)	C_2H_5OH/H_2O	TEA	28000	311 h^{-1}	11.5 (420 nm)	145
CdSe	**21**	520 nm (LED)	H_2O	AA	280000			146

[a] CaI: clostridium acetobutylicum [FeFe]-hydrogenase I, PAA: poly(acrylic acid), PEI: polyethylenimone, DHLA: dihydrolipoic acid.
[b] TH: tungsten halogen lamp, Hg: mercury lamp, Xe: xenon lamp.
[c] TEOA: triethanolamine, AA: ascorbic acid, TEA: triethylamine

Table 3 photocatalyst systems containing CdX and carbon-based materials for photocatalytic H_2 produciton.

Photocatalyst	Optimized mass fraction of carbon-based material	Cocatalyst	Light source[a]	Aqueous reaction solution[b]	H_2 evolution			Ref.
					Activity ($\mu molh^{-1}g^{-1}$)	QE (%)	Enhancement Factor[c]	
MWCNTs/CdS	10 wt%		λ ≥ 420 nm (Xe)	0.25 M Na_2SO_3 + 0.35 M Na_2S	4977	2.16 (420 nm)	1.8	181
CNTs/$Cd_{0.1}Zn_{0.9}S$	0.25 wt%		λ ≥ 420 nm (Xe)	0.25 M Na_2SO_3 + 0.35 M Na_2S	1564	7.9 (420 nm)	3.2	183
$Zn_{0.83}Cd_{0.17}S$/ CNTs			300~800 nm(Xe)	0.02 M Na_2SO_3 + 0.1 M Na_2S	6030		1.5	184
CdS/CNTs	4wt%	0.75wt% NiS	λ >420 nm (Xe)	0.25 M Na_2SO_3 + 1.0 M Na_2S	12130		15	186
$Zn_{0.83}Cd_{0.17}S$/ CNTs	0.25wt%		500 W Xe lamp	0.02 M Na_2SO_3 + 0.1 M Na_2S	5410		1.3	187
CdS/RGO	1 wt%	0.5wt% Pt	λ ≥ 420 nm (Xe)	10vol% lactic acid	56000	22.5 (420 nm)	45.6	188
CdS/GO	5 wt%		λ ≥ 420 nm (Xe)	0.25 M Na_2SO_3 + 0.35 M Na_2S	3140	4.8 (420nm)	1.3	189
CdS/RGO	10 wt%		λ ≥ 420 nm (Xe)	0.25 M Na_2SO_3 + 0.35 M Na_2S	4200	10.4(420nm)	1.5	190
CdS/RGO	1wt%		λ ≥ 420 nm (Xe)	0.05 M Na_2SO_3 + 0.1 M Na_2S	700		4.8	191
CdS-MoS_2/ graphene	1.33wt%	0.67wt% MoS_2	λ ≥ 420 nm (Xe)	20vol% lactic acid	9000	28.1(420 nm)	72	192
CdS-Al_2O_3/GO	1wt%		500W phoenix tungsten halogen lamp	0.25 M Na_2SO_3 + 0.35 M Na_2S	1750	14(420 nm)	4.2	193
CdS-ZnO/GO	1wt%		500W phoenix tungsten halogen lamp	0.25 M Na_2SO_3 + 0.35 M Na_2S	3755	30(420 nm)	9.0	193
CdS-ZnO/RGO	2wt%		300 W Xe lamp	0.1 M Na_2SO_3 + 0.1 M Na_2S	5100		34.0	194
CdS-TaON/RGO	1wt%	0.4wt% Pt	λ ≥ 420 nm (Xe)	0.04 M Na_2SO_3 + 0.1 M Na_2S	3165	31(420 nm)		195
CdS QDs - $ZnIn_2S_4$/RGO	1wt%	0.4wt% Pt	λ ≥ 420 nm (Xe)	0.04 M Na_2SO_3 + 0.1 M Na_2S	27000	56(420 nm)		196
$Zn_{0.8}Cd_{0.2}S$/RGO	0.25wt%		AM 1.5G (Xe)	0.25 M Na_2SO_3 + 0.35 M Na_2S	1824	23.4(420 nm)	4.5	197
CdS/N-doped graphene	2wt%		λ ≥ 420 nm (Xe)	0.1 M Na_2SO_3 + 0.1 M Na_2S	1050		5.3	198
CdS/sulfonated graphene	2 wt%		Metal halide lamp, λ ≥ 380 nm	0..07M Na_2SO_3 + 0.05 M Na_2S	166			199
CdS/cysteine-Modified RGO	0.7 wt%	2.1wt% Pt	λ ≥ 420 nm (Xe)	10vol% lactic acid	29861	50.7(420 nm)		200
CdS/RGO	5 wt%	0.5wt% Pt	λ ≥ 420 nm (Xe)	1.25 M $(NH_4)_2SO_3$	29400		7.3	202
g-C_3N_4/CdS	1 wt%	1 wt% Pt	λ ≥ 420 nm (Xe)	0.25 M Na_2SO_3 + 0.35 M Na_2S	5303	3.6 (420 nm)	2.5	208
CdS-g-C_3N_4	88 wt%	0.5 wt% Pt	λ ≥ 420 nm (Xe)	0.1 M AA	4494	8.0 (420 nm)	1.8	204
g-C_3N_4–CdS	85 wt%	9 wt% NiS	λ ≥ 420 nm (Xe)	10 vol% TEOA	2563		4.4	209
CdS-g-C_3N_4	2 wt%	0.6 wt% Pt	λ ≥ 420 nm	0.25 M	4152	4.3 (420 nm)	2	205

	(Xe)	Na_2SO_3 + 0.35 M Na_2S

[a] Xe: xenon lamp. [b]TEOA: triethanolamine, AA: ascorbic acid.
[c]Enhancement factor refers to the enhancing times of photocataly H2 generation rate of photocatalyst system containing CdX and carbon-based materials, compared to pure CdX photocatalyst.